Chapter 1

Inference models to estimate network characteristics

The first chapter of the thesis is concerned with adaptive unicast applications that adjust their sending rate in order to avoid congestion in the network. One way of achieving this involves estimating both the available bandwidth and the available storage capacity along a connection. The research presented herein builds on simple inference models based on finite capacity single server queues to estimate the buffer size, the intensity of cross traffic and the service rate at the bottleneck link of a path between two application-level hosts. Throughout the chapter, several groups of moment-based estimators are proposed to estimate these quantities. The best scheme, identified as the one achieving the best performance and the fastest convergence, is then identified through simulation. An application to routing in content distribution networks is discussed.

Keywords: Queueing, $M/M/1/K$ queue, $M/D/1/K$ queue, measurement, monitoring, simulation.

Note: Part of the material presented in this chapter is published in [16].

1.1 Introduction

The huge expansion of the Internet coupled with the emergence of new (in particular, multimedia) applications pose challenging problems in terms of performance and control of the network. These include the design of efficient congestion control and recovery mechanisms, and the ability of the network to offer good Quality of Service (QoS) to the users. In the current Internet, there is a single class of best effort service which does not promise anything to the users in terms of performance guarantees. The forthcoming deployment in the Internet of differentiated services (known as DiffServ [1]) will be a first (long awaited) step towards the support of various types of applications and business requirements. It is however doubtful that DiffServ – which will mark each packet to receive a particular forwarding treatment, or per-hop behavior, at each network node – or the RED mechanism for congestion avoidance in gateways [53] alone will solve all QoS issues raised by real-time applications. Diffserv and RED are two instances of a general approach that aims at adding more intelligence in the *network*. A more ambitious component of this approach is captured in the concept of *active networking* [122] that aims at exploiting mobile code and programmable infrastructure to provide rapid and specialized service introduction.

A complementary approach for providing QoS guarantees is to add intelligence to the *applications*. The idea is to provide applications with enough knowledge of the network so that they can use this information to adapt their transmission rates to current network conditions. Since it is impossible to monitor every link on the Internet, static (e.g. bandwidth of a link) and dynamic (e.g. available bandwidth on a path) network internal characteristics have to be estimated from measurements delivered by the network (e.g. packet losses in RTCP feedback). Our work falls into the latter category.

In this chapter, we are interested in the *available* bandwidth on a route. Under the single bottleneck link assumption, we expect this quantity to be better estimated if one has estimates of the bottleneck bandwidth, the cross traffic intensity and the buffer size at the bottleneck link. The latter quantities are not provided by *packet pair* algorithms [73, 21, 31, 94, 77]). We believe that the available bandwidth will be better estimated when taking explicitly into account the cross traffic and the buffer size at the bottleneck link. Not only can the application adapt its sending rate and/or encoding in response to network congestion, but it can estimate the maximum size of a burst of packets as well. We propose to perform active measurements by probing the network, and model the end-to-end path as a simple single server queueing model with two input streams: the probe stream and the cross traffic stream (also called the background traffic stream). The input probe traffic will be a Poisson process and the input cross traffic will be *assumed* to be a Poisson process. Two models will be considered depending on whether the service times are assumed to be exponentially distributed or deterministic. Based on the single bottleneck link assumption, the inference models will allow us to simultaneously estimate the bandwidth capacity, the background traffic intensity and the buffer size at the bottleneck link. Potential applications for this work are: adapting the transmission for congestion control [21, 111], load balancing

in routers and analysis of IP network usage. In fact, ISPs need bandwidth monitoring tools to plan their capacity upgrades, and to detect congested or underutilized links [26].

The chapter is organized as follows. Section 1.2 briefly discusses some related works and Section 1.3 introduces the methodology followed in this work. Two inference models based on the $M/M/1/K$ and the $M/D/1/K$ queues are introduced in Sections 1.4 and 1.5, respectively. In each case, several QoS metrics of interest are identified and expressed in terms of the parameters to be estimated (buffer size, cross traffic intensity, server capacity). In Section 1.6, we propose ten schemes that can be used to estimate these quantities, and under the assumption that the service capacity is known (provided for instance by a packet pair technique), we propose a total of eleven schemes that can be used to compute estimates of the intensity of the cross traffic and the buffer size. Section 1.7 reports simulation results obtained with the `ns-2` simulator [83] from which we were able to select the best scheme out of the proposed schemes. Extensions to our work are given in Section 1.8.

1.2 Related work

Inference models have been widely used for characterizing internal network behavior from end-to-end multicast measurements. This methodology is captured in the MINC project [3]. Among the network characteristics which have been estimated (refer to [3] for a list of references), are the internal loss rates in the MBone [29, 28, 30, 51], the packet delay variance at interior network links [50], the network-internal delay [100, 49], and the multicast topology [27, 48, 47] (these lists are not exhaustive).

The estimation of network characteristics from measurements has been carried out in a number of cases. For instance, the arrival rates of interfering traffic and the service rates of customers on the route of a CAC (call acceptance controller) probe stream can be estimated for a product form Kelly network [110]. The steady-state throughput of a bulk transfer TCP flow can be estimated as a function of loss rate and round-trip time using the so-called TCP-friendly formula [93, 80, 82]. The packet pair technique can be used to estimate both the bottleneck bandwidth [21, 31, 94, 77] and the available bandwidth along a path connecting two hosts on the Internet [67, 73, 31]. Although the previous estimates have been devised under the assumption that a single bottleneck link exists on a path connecting two hosts, experiments reported in the previous references indicate that these estimates still perform reasonably well when this assumption is violated.

The estimation of the bottleneck bandwidth has been carefully investigated by Paxson [94, Chapter 14]. Paxson proposes a robust procedure called "packet bunch mode" (PBM) and compares the results returned by PBM with other techniques such as receiver-based packet pair (RBPP), sender-based packet pair (SBPP) and peak rate (PR). It is seen in [94] that PR performs poorly, that RBPP performs as well as PBM if some requirements are observed and that SRPP does not work especially well (the estimators studied in [21, 31] are both sender-based). As for PBM, Paxson observes that "*it produces many bandwidth*

estimates that accord with known link speeds, and produces few erroneous results, except for a tendency to misdiagnose a multiple-channel bottleneck link in presence of considerable delay noise". Note that PBM has a large component of heuristics, as it has to deal with the multimodal distribution of bandwidth measurements to further identify and select the capacity estimate from these modes.

Subsequent to our work, Lai and Baker [77] propose another technique called "receiver only packet pair" (ROPP), which is yet another variant of the packet pair algorithm. The authors compare the performance of ROPP and SRPP and RBPP (but not PBM). The results reported in [77] suggest that ROPP can achieve an accuracy close to that of RBPP, while maintaining the ease of deployment of SBPP. Recently, Dovrolis, Ramanathan and Moore [46] develop a bandwidth estimation methodology that is robust to cross traffic effects. This methodology, based on end-to-end measurements, is implemented in a tool called *pathrate*. There are potentially two phases in *pathrate*. In the first phase, a packet pair probing is done. If the distribution of bandwidth measurements is unimodal, then the unique mode is the bandwidth estimator and the measurement process terminates. Otherwise (multimodal distribution), the second phase is initiated and a packet train probing is done. The authors make use of a heuristic to estimate the bottleneck bandwidth. When evaluating the heuristic rule, they observe that the methodology is quite accurate as long as the path capacity is lower than about 40 Mbps. For higher capacities, the estimator underestimates the capacity, in some cases by a factor of almost two. However, the authors show that the performance of their estimator is enhanced when increasing the *histogram bin width* ω. This parameter tunes the resolution of the estimator, for instance, if $\omega = 2$ then *pathrate* will output estimates at 2 Mbps interval (refer to [46] for more details).

1.3 Methodology

Consider the following scenario: an application sends a probe stream into the network together with its data packets. All packets are assumed to follow the same path to the destination. At the source, the arrival times to the network (denoted by a_n) are available. At the destination, the departure times from the network (denoted by d_n) are available as well as the information on lost packets and on packets that find the network non-empty. Assume that all these variables are available at the source by using some feedback mechanism. The source is then capable of estimating some QoS related metrics such as the loss probability or the expected response time of the network.

Given a model for the network (such as a simple single server queue representing the bottleneck node along the path source-destination), one is able to express the QoS related metrics in terms of the buffer size, the cross traffic intensity and the server capacity. Given estimates of these QoS related metrics, the source can simply infer the values of the buffer size, the cross traffic intensity and the server capacity, by using the network model. Figure 1.1 illustrates the estimation approach just described.

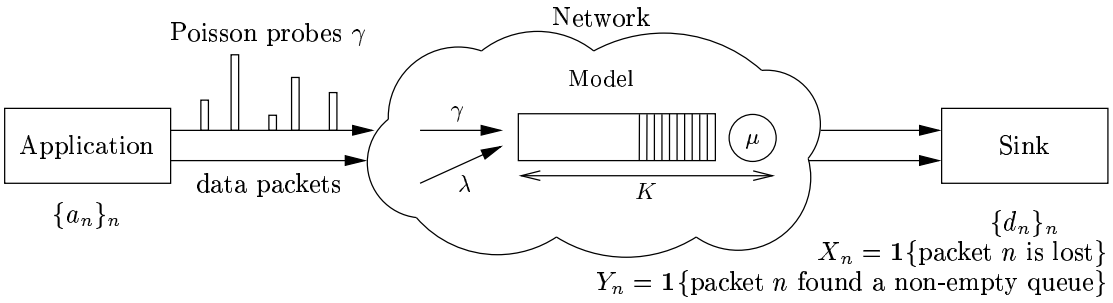

General methodology:

- collect at the source samples of the variables a_n, d_n, X_n, Y_n,
- estimate some performance metrics using these variables (e.g. loss probability),
- given a model for the connection, express these metrics in terms of the parameters to estimate,
- infer the unknown parameters.

Figure 1.1: The methodology

1.4 The $M+M/M/1/K$ queue

1.4.1 The model

We model an Internet connection by a single server queue representing its bottleneck node, following [22]. The buffer is finite with room for K customers ($K \geq 1$) including the customer in service. The incoming traffic at the bottleneck is modeled as two independent Poisson sources: the probe traffic generated by a foreground source with rate γ, and the cross traffic generated by a background source with rate λ. This background source can be seen as the superposition of many heterogeneous sources. We model the service times as i.i.d. random variables with exponential distribution with mean $1/\mu$, furthermore, independent of the arrival processes. This assumption represents the variability of the packet sizes. We are aware of the strength of this assumption, but we assume it for the tractability it gives to the study of the model.

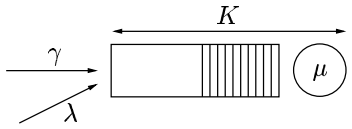

Figure 1.2: The inference model

The traffic intensity is defined as

$$\rho = \frac{\lambda + \gamma}{\mu}. \tag{1.1}$$

We are interested in the behavior of the system from the perspective of the foreground customers. This includes stationary measures such as expected delay, loss probability, server

occupancy and a number of additional statistics associated with the foreground loss process, namely, the probability of two consecutive losses and the probability of two consecutive successes. It is important to observe that these stationary metrics do not pertain exclusively to the foreground source, but to the background source as well, due to the Poisson assumption and its memoryless property.

Let $\{Q_n\}_{n=1}^{\infty}$ be the process of the number of packets in the buffer at time of the nth arrival from foreground source, and let $Q = \lim_{n\to\infty} Q_n$[1]. The distribution of Q is $\pi_i = P(Q = i)$. It is known that [75]

$$\pi_i = \frac{(1-\rho)\rho^i}{1-\rho^{K+1}}, \qquad i = 0, 1, \ldots, K. \tag{1.2}$$

1.4.2 The loss probability

We focus here on the loss process. We define $X_n = \mathbf{1}\{Q_n = K\}$ and $X = \lim_{n\to\infty} X_n$. A customer is lost whenever it arrives to a full buffer. In other words, customer n is lost whenever $X_n = 1$ and is not lost otherwise. Let $\{a_n\}_{n=1}^{\infty}$ and $\{d_n\}_{n=1}^{\infty}$ be the arrival times to the system and the departure times from the system, respectively, of the nth foreground customer, $n = 1, 2, \ldots$. When a packet is lost, it never reaches the destination. We shall assume that $d_n = \infty$ if $X_n = 1$.

Using the PASTA property [17, page 137], the probability that a foreground customer arrives to find the system full and is lost is

$$\begin{aligned} P_L := P(X = 1) &= P(Q = K) \\ &= \frac{(1-\rho)\,\rho^K}{1-\rho^{K+1}}. \end{aligned} \tag{1.3}$$

Observe that the expression for P_L can be used to give the following expression for K in terms of ρ and P_L,

$$K = \frac{1}{\log\rho} \log\left(\frac{P_L}{1-\rho\,(1-P_L)}\right). \tag{1.4}$$

1.4.3 The server utilization

The second metric of interest is the utilization U of the server, defined as the probability of a non-empty queue as seen by a foreground customer. In order to express U, we

[1] A word on the notation in use: let $\{Z_n\}_n$ be a sequence of random variables taking values in $[0, \infty)$. Assume that $\lim_{n\to\infty} P[Z_n \le x]$ exists for all $x \ge 0$. Then $Z = \lim_{n\to\infty} Z_n$ designates any random variable such that $P[Z \le x] = \lim_{n\to\infty} P[Z_n \le x]$

introduce the following indicator $Y_n = \mathbf{1}\{Q_n > 0\}$ and define $Y = \lim_{n\to\infty} Y_n$. The server utilization is then

$$\begin{aligned} U := P(Y=1) &= P(Q>0) \\ &= \rho\left(\frac{1-\rho^K}{1-\rho^{K+1}}\right) \qquad (1.5) \\ &= \rho\,(1-P_L). \qquad (1.6) \end{aligned}$$

Again, we can derive from the expression for U the following expression for K in terms of ρ and U,

$$K = \frac{1}{\log\rho}\log\left(\frac{1-U/\rho}{1-U}\right). \qquad (1.7)$$

1.4.4 The expected response time

When available, the expected response time is also a relevant metric. To express this quantity, we first define T_n as the response time of the nth foreground packet. It follows that $T_n = d_n - a_n$. Again, let $T = \lim_{n\to\infty} T_n$, then, the expected response time is

$$R := E[\,T \mid X = 0\,] = \frac{\sum_{i=0}^{K-1}(i+1)\,\pi(i)}{\mu(1-\pi_K)} \qquad (1.8)$$

since a customer waits for an average time $(i+1)/\mu$ if there were already i customers in the queue; $1-\pi_K$ is the probability of a success. Using (1.2) we can write

$$R = \frac{1}{\mu\,(1-\pi_K)}\left(\frac{1-\rho}{1-\rho^{K+1}}\sum_{i=0}^{K-1}(i+1)\,\rho^i\right).$$

Hence,

$$\begin{aligned} R &= \frac{1}{\mu\,(1-\pi_K)}\left[\frac{1-\rho^K}{(1-\rho)\,(1-\rho^{K+1})} - \frac{K\,\rho_K}{1-\rho^{K+1}}\right] \\ &= \frac{1}{\mu\,(1-\rho)} - \frac{K}{\mu}\,\frac{\pi_K}{(1-\rho)\,(1-\pi_K)}. \qquad (1.9) \end{aligned}$$

The last expression for R, which was derived using (1.2), will prove useful. We can express R only in terms of ρ and K by replacing π_K given by (1.3) in (1.9). This gives

$$R = \frac{1}{\mu\,(1-\rho)} - \frac{K}{\mu}\,\frac{\rho^K}{1-\rho^K}. \qquad (1.10)$$

1.4.5 The conditional loss probability

The next metric we are going to study is the conditional loss probability or, in other words, the probability that two consecutive losses occur. It is expressed as follows

$$q_L := P(Q_n = K \mid Q_{n-1} = K). \tag{1.11}$$

In order to be able to derive a closed form expression for q_L, we define $N(t)$ to be the queue length of the system at time $t \geq 0$ with the foreground source removed ($\gamma = 0$). Let $P_{i,k}(t) = P(N(t) = k \mid N(0) = i)$. Hence (1.11) rewrites

$$q_L = \gamma \int_0^\infty e^{-\gamma t} P_{K,K}(t)\, \mathrm{d}t = \gamma\, P^*_{K,K}(\gamma) \tag{1.12}$$

where $P^*_{K,K}(\gamma)$ is the Laplace transform of $P_{K,K}(t)$.

Proposition 1.4.1

$$P^*_{i,K}(\gamma) = \frac{a^{i+1}\,(1-a)^{-1} - b^{i+1}\,(1-b)^{-1}}{\lambda\,(b^{K+1} - a^{K+1})}$$

for $i = 0, 1, \ldots, K$, *where*

$$a = \frac{\lambda + \mu + \gamma + \sqrt{(\lambda+\mu+\gamma)^2 - 4\lambda\mu}}{2\lambda}$$
$$b = \frac{\lambda + \mu + \gamma - \sqrt{(\lambda+\mu+\gamma)^2 - 4\lambda\mu}}{2\lambda}.$$

♦

Proof. Recall the definition $P_{i,k}(t) = P(N(t) = k \mid N(0) = i)$ where $N(t)$ is the queue length of the system with the foreground source removed ($\gamma = 0$) at time $t \geq 0$. We have the following differential equations:

$$\frac{\mathrm{d}}{\mathrm{d}t} P_{i,0}(t) = -\lambda P_{i,0}(t) + \mu P_{i,1}(t) \tag{1.13}$$
$$\frac{\mathrm{d}}{\mathrm{d}t} P_{i,K}(t) = -\mu P_{i,K}(t) + \lambda P_{i,K-1}(t) \tag{1.14}$$
$$\frac{\mathrm{d}}{\mathrm{d}t} P_{i,k}(t) = -(\lambda+\mu) P_{i,k}(t) + \lambda\, P_{i,k-1}(t) + \mu\, P_{i,k+1}(t), \text{for } k = 1, \ldots, K-1, \tag{1.15}$$

for $i = 0, \ldots, K$. Define $P_i(z,t) = \sum_{k=0}^K P_{i,k}(t) z^k$. Then,

$$z \frac{\mathrm{d}}{\mathrm{d}t} P_i(z,t) \;=\; z \frac{\mathrm{d}}{\mathrm{d}t} \sum_{k=0}^K P_{i,k}(t) z^k \;=\; z \sum_{k=0}^K \frac{\mathrm{d}}{\mathrm{d}t} P_{i,k}(t) z^k.$$

Using (1.13) – (1.15) and after some algebra we get

$$\frac{z}{1-z}\frac{\mathrm{d}}{\mathrm{d}t}P_i(z,t) = (\mu-\lambda z)P_i(z,t) - \mu P_{i,0}(t) + \lambda z^{K+1}P_{i,K}(t). \tag{1.16}$$

Now we consider the Laplace transform of $P_i(z,t)$, $P_i^*(z,s) = \int_0^\infty e^{-st}P_i(z,t)\,\mathrm{d}t$. Replacement of this in (1.16) along with the use of the following relation

$$\int_0^\infty e^{-st}\frac{\mathrm{d}}{\mathrm{d}t}\,P_i(z,t)\,\mathrm{d}t = sP_i^*(z,s) - P_i(z,0)$$

and some algebraic manipulations yields

$$P_i^*(z,s) = \frac{z^{i+1} - \mu(1-z)P_{i,0}^*(s) + \lambda(1-z)z^{K+1}P_{i,K}^*(s)}{sz-(1-z)(\mu-\lambda z)} \tag{1.17}$$

where $P_{i,k}^*(s) = \int_0^\infty e^{-st}P_{i,k}(t)\mathrm{d}t$, $k = 0,1,\ldots,K$. The denominator of the right-hand side of (1.17) contains two zeros,

$$z_1(s) = \frac{\lambda+\mu+s-\sqrt{(\lambda+\mu+s)^2-4\lambda\mu}}{2\lambda}$$
$$z_2(s) = \frac{\lambda+\mu+s+\sqrt{(\lambda+\mu+s)^2-4\lambda\mu}}{2\lambda}$$

for $\Re(s) \geq 0$.

As $P_i^*(z,s)$ is analytic, the zeros of the denominator must also be zeros of the numerator. More precisely, the numerator must satisfy

$$z_k^{i+1}(s) - [1-z_k(s)][\mu P_{i,0}^*(s) - \lambda z_k(s)^{K+1}P_{i,K}^*(s)] = 0.$$

These two equations for $k = 1,2$ can be solved to yield

$$P_{i,0}^*(s) = \frac{z_2(s)^{i+1}z_1(s)^{K+1}/[1-z_2(s)] - z_1(s)^{i+1}z_2(s)^{K+1}/[1-z_1(s)]}{\mu\left(z_1(s)^{K+1} - z_2(s)^{K+1}\right)}$$
$$P_{i,K}^*(s) = \frac{z_2(s)^{i+1}/[1-z_2(s)] - z_1(s)^{i+1}/[1-z_1(s)]}{\lambda\left(z_1(s)^{K+1} - z_2(s)^{K+1}\right)}.$$

Let a and b be defined as $a = z_2(\gamma)$ and $b = z_1(\gamma)$, we get

$$P_{i,K}^*(\gamma) = \frac{a^{i+1}(1-a)^{-1} - b^{i+1}(1-b)^{-1}}{\lambda\left(b^{K+1}-a^{K+1}\right)}$$

and the proof is concluded. ■

From Proposition 1.4.1 we get that

$$P^*_{K,K}(\gamma) = \frac{(1-a)^{-1} - (b/a)^{K+1}(1-b)^{-1}}{\lambda\left((b/a)^{K+1} - 1\right)}$$

which in turn implies from (1.12) that

$$q_L = \left(\frac{\gamma}{\lambda}\right)\left(\frac{(1-a)^{-1} - (b/a)^{K+1}(1-b)^{-1}}{(b/a)^{K+1} - 1}\right). \tag{1.18}$$

Expression (1.18) for q_L can be inverted to give

$$K = \frac{\log\left(\frac{\gamma}{1-a} + q_L\lambda\right) - \log\left(\frac{\gamma}{1-b} + q_L\lambda\right)}{\log b - \log a} - 1. \tag{1.19}$$

1.4.6 The conditional non-loss probability

Another metric can also be calculated. It is the conditional probability that an arriving foreground packet finds room in the buffer given that the previous foreground customer was also admitted. We shall refer to this probability as the *c*onditional non-loss probability and will denote it by q_N. We have

$$\begin{aligned}
q_N &:= P(Q_{n+1} \neq K \,|\, Q_n \neq K) \\
&= \sum_{i=0}^{K-1} \frac{P(Q_{n+1} \neq K, Q_n = i, Q_n \neq K)}{P(Q_n \neq K)} \\
&= \sum_{i=0}^{K-1} \frac{P(Q_{n+1} \neq K \,|\, Q_n = i)\,\pi(i)}{1 - \pi(K)} \\
&= \sum_{i=0}^{K-1} \frac{(1 - P(Q_{n+1} = K \,|\, Q_n = i))\,\pi(i)}{1 - \pi(K)}.
\end{aligned}$$

Recall the definition of $P_{i,k}(t) = P(N(t) = k \,|\, N(0) = i)$, where $N(t)$ is the queue-length at time t when $\gamma = 0$ (no foreground customers). Since the nth foreground customer is accepted in the system when $Q_n = i < K$, we have

$$\begin{aligned}
P(Q_{n+1} = K \,|\, Q_n = i) &= \int_0^\infty P_{i+1,K}(t)\,\gamma\, e^{-t\gamma}\,\mathrm{d}t \\
&= \gamma\, P^*_{i+1,K}(\gamma)
\end{aligned}$$

for $i = 0, 1, \ldots, K-1$, with $P^*_{j,k}(s) = \int_0^\infty e^{-st} P_{j,k}(t)\mathrm{d}t$. Therefore,

$$q_N = 1 - \gamma \sum_{i=0}^{K-1} \frac{P^*_{i+1,K}(\gamma)\,\pi(i)}{1 - \pi(K)}. \tag{1.20}$$

Using Proposition (1.4.1) which gives an expression for $P^*_{j,K}(\gamma)$, (1.20) rewrites

$$q_N = 1 - \left(\frac{\gamma}{\lambda}\right)\left(\frac{1-\rho}{1-\rho^K}\right)\left(\frac{1}{b^{K+1}-a^{K+1}}\right)\left[\frac{a^2\left(1-(\rho a)^K\right)}{(1-a)(1-\rho a)} - \frac{b^2\left(1-(\rho b)^K\right)}{(1-b)(1-\rho b)}\right]. \quad (1.21)$$

Since

$$P(Q_{n+1}=K) = P\Big(Q_{n+1}=K|Q_n=K\Big)P(Q_n=K)+P\Big(Q_{n+1}=K|Q_n\neq K\Big)P(Q_n\neq K)$$

we deduce that P_L, q_L and q_N are linked by the following relationship

$$P_L\left(1-q_L\right) = \left(1-P_L\right)\left(1-q_N\right). \quad (1.22)$$

1.5 The $M+M/D/1/K$ queue

1.5.1 The model

We still consider the model introduced in Section 1.4.1 but we now change the assumption that the service times are exponentially distributed. Instead we will assume that the service times are constant and all equal to $1/\mu$. In Section 1.4.1, we motivated our choice for exponentially distributed service times by the fact that various packet lengths are possible. Taking into consideration that packet lengths may not be so variable to justify the choice of an exponential distribution, we study here another case: the service times are taken to be constant (i.e. all packets have the same length) with value $\sigma = 1/\mu$. Recall the definition of the traffic intensity given in (1.1).

Again, let $\{Q_n\}_{n=1}^{\infty}$ be the process of the number of packets in the queue at time of the nth arrival from foreground source and let $Q = \lim_{n\to\infty} Q_n$. Some preliminary results must be introduced before computing the stationary distribution of Q.

Let $\mathcal{F}(\theta) = E[\exp(-\theta\sigma)]$ $(\Re(\theta)\geq 0)$ be the Laplace–Stieltjes transform (LST) of the service time distribution. Since we consider a constant service time, this transform rewrites as $\mathcal{F}(\theta) = \exp(-\theta\sigma)$. For $\rho > 0$ and $|z| \leq 1$, define

$$\begin{aligned}\mathcal{G}_\rho(z) &= \mathcal{F}\left(\frac{\rho\left(1-z\right)}{\bar{\sigma}}\right) - z \\ &= e^{-\rho\left(1-z\right)} - z. \end{aligned} \quad (1.23)$$

For $\rho > 0$, we denote by $z_0(\rho)$ the zero of $\mathcal{G}_\rho(z)$ having the smallest modulus. Also, we denote by $[z^n]f$ the coefficient of z^n in the Taylor series expansion of f.

To express the stationary distribution of Q, we base our calculus on Cohen's analysis of the $M/G/1$ queue with finite waiting room $(K > 1)$ [39, Chapter III.6]. Introduce the

parameter B defined as

$$B = 1 + \frac{\rho}{2\pi i} \oint_{D_r} \left(\frac{1}{\mathcal{G}_\rho(z)} \right) \frac{\mathrm{d}z}{z^{K-1}} \tag{1.24}$$

with D_r any circle in the complex plane with center 0 and radius strictly less than $|z_0(\rho)|$. According to the results obtained by Cohen [39, page 575], we have

$$P(Q=0) = \frac{1}{B}, \tag{1.25}$$

$$P(Q=j) = \frac{1}{2\pi i B} \oint_{D_r} \left(\frac{1-z}{\mathcal{G}_\rho(z)} - 1 \right) \frac{\mathrm{d}z}{z^j}, \text{ for } j = 1, \ldots, K-1, \tag{1.26}$$

$$P(Q=K) = \frac{1}{2\pi i B} \oint_{D_r} \left(\frac{\rho - 1}{\mathcal{G}_\rho(z)} + \frac{1}{1-z} \right) \frac{\mathrm{d}z}{z^{K-1}}. \tag{1.27}$$

The integrals in the r.h.s. of (1.24), (1.26) and (1.27) can be evaluated using the theorem of residues [118]. More precisely, the formula which is to be used is

$$\oint_C f(z)\mathrm{d}z = 2\pi i \sum_{k=1}^{n} \mathrm{Res}[f, z_k]$$

where $(z_1, \ldots, z_n)$ are the poles of the meromorphic function[2] f inside the circle C. To calculate a residue, use the identity

$$\mathrm{Res}[f, z_k] = \frac{1}{(m-1)!} \left(\frac{\mathrm{d}^{(m-1)}}{\mathrm{d}z^{m-1}} (z - z_k)^m f(z) \right)_{z=z_k} = [z^{m-1}](z - z_k)^m f(z)$$

where m is the multiplicity of pole z_k. It is easily seen that

$$\frac{1}{2\pi i} \oint_{D_r} \frac{1}{z^j}\,\mathrm{d}z = \mathrm{Res}\left[\frac{1}{z^j}, 0\right] = [z^{j-1}]1 = \begin{cases} 1, & \text{if } j = 1 \\ 0, & \text{if } j = 2, 3, \ldots \end{cases}$$

$$\frac{1}{2\pi i} \oint_{D_r} \frac{1}{(1-z)\, z^{K-1}}\,\mathrm{d}z = \mathrm{Res}\left[\frac{1}{(1-z)z^{K-1}}, 0\right] = [z^{K-2}]\frac{1}{1-z} = 1,$$

$$\frac{1}{2\pi i} \oint_{D_r} \frac{1}{\mathcal{G}_\rho(z)\, z^{j-1}}\,\mathrm{d}z = \mathrm{Res}\left[\frac{1}{\mathcal{G}_\rho(z)\, z^{j-1}}, 0\right] = \begin{cases} 0, & \text{if } j = 1 \\ [z^{j-2}]\frac{1}{\mathcal{G}_\rho(z)}, & \text{if } j = 2, 3, \ldots \end{cases}$$

Finally, from (1.24)–(1.27) and with the help of the previous identities, the distribution of

[2] A meromorphic function is a rational function, i.e. it has no essential singular points; for instance $f(z) = e^{(1/z)}$ is not a meromorphic function since 0 is a singular essential point.

Q is given by

$$\pi_0 = \frac{1}{1+\rho\,\alpha_K(\rho)}, \tag{1.28}$$

$$\pi_1 = \frac{\alpha_2(\rho)-1}{1+\rho\,\alpha_K(\rho)}, \tag{1.29}$$

$$\pi_j = \frac{\alpha_{j+1}(\rho)-\alpha_j(\rho)}{1+\rho\,\alpha_K(\rho)}, \quad j=2,\ldots,K-1, \tag{1.30}$$

$$\pi_K = \frac{1+(\rho-1)\,\alpha_K(\rho)}{1+\rho\,\alpha_K(\rho)}, \tag{1.31}$$

where we have defined

$$\alpha_j(\rho) := [z^{j-2}]\frac{1}{\mathcal{G}_\rho(z)} = \frac{1}{(j-2)!}\left(\frac{\mathrm{d}^{(j-2)}}{\mathrm{d}z^{j-2}}\,\frac{1}{\mathcal{G}_\rho(z)}\right)_{z=0} = \frac{1}{2\pi i}\oint_{D_r}\frac{1}{\mathcal{G}_\rho(z)\,z^{j-1}}\,\mathrm{d}z. \tag{1.32}$$

When the service times are constant, an analytical expression for $\alpha_j(\rho)$ can be derived. To this end, start from

$$\frac{1}{\mathcal{G}_\rho(z)} = \frac{1}{e^{-\rho\,(1-z)}-z} = e^{\rho\,(1-z)}\sum_{i\geq 0}(ze^{\rho\,(1-z)})^i$$

where the last equality is true for z such that $|ze^{\rho\,(1-z)}|<1$, which yields

$$\begin{aligned}\frac{1}{\mathcal{G}_\rho(z)} &= \sum_{i\geq 0} z^i e^{\rho\,(i+1)}\,e^{-\rho\,(i+1)z} = \sum_{i\geq 0}\sum_{k\geq 0} z^i e^{\rho\,(i+1)}\,\frac{(-\rho\,(i+1)z)^k}{k!}\\ &= \sum_{n\geq 0}\left(\sum_{i+k=n}\frac{e^{\rho\,(i+1)}\,(-1)^k\,\rho^k\,(i+1)^k}{k!}\right)z^n.\end{aligned}$$

Hence,

$$\alpha_j(\rho) = \sum_{i+k=j-2}\frac{e^{\rho\,(i+1)}(-1)^k\rho^k(i+1)^k}{k!} = \sum_{k=0}^{j-2}\frac{e^{\rho\,(j-k-1)}\,(-1)^k\,\rho^k\,(j-k-1)^k}{k!},\ j\geq 2. \tag{1.33}$$

1.5.1.1 Alternative computation of $\alpha_j(\rho)$

Computing $\alpha_j(\rho)$ as in (1.33) becomes rapidly intractable because of the factorial in the denominator. An alternative calculation consists of computing the integral in (1.32). The key point is to determine $r<r_0:=|z_0(\rho)|$, the radius of the circle over which the integral is to be computed. Recall that $z_0(\rho)$ is the zero of $\mathcal{G}_\rho(z)$ having the smallest modulus. For general service times, it is known from the Lemma of Takàcs [114, pages 47-49] that:

- $z_0(\rho)$ is a continuous function of ρ,
- $z_0(\rho) = 1$ if $\rho \leq 1$,
- $z_0(\rho) < 1$ if $\rho > 1$,
- $z_0(\rho)$ is the only zero inside the unit circle if $\rho > 1$,
- for $\rho = 1$, the multiplicity of the zero $z_0(1) = 1$ is 2.

When the service times are deterministic, the zeros of $\mathcal{G}_\rho(z)$ are simply a Lambert W series. For later use, we briefly review some of the properties of the Lambert W function [40]. By definition, the Lambert W function satisfies:

$$W(x)e^{W(x)} = x.$$

As this equation has an infinite number of solutions for each (non-zero) value of x, $W(x)$ has an infinite number of branches. Denote the kth branch by $W_k(x)$. If x is real, then for $-1/e \leq x < 0$, there are two possible (negative) *real* values of $W(x)$. The branch satisfying $-1 \leq W(x) < 0$ is denoted by $W_0(x)$ and referred to as the principal branch of the W function; and the branch satisfying $W(x) \leq -1$ is denoted by $W_{-1}(x)$. Note that $W_0(x)$ and $W_{-1}(x)$ are the only branches that take on real values and that $W_0(-1/e) = W_{-1}(-1/e) = -1$.

Let us now return to the function $\mathcal{G}_\rho(z)$. Rewriting it as follows:

$$\mathcal{G}_\rho(z) = -\frac{e^{\rho z}}{\rho}\Big(- \rho e^{-\rho} + \rho z e^{-\rho z}\Big),$$

it becomes clear that the zeros of $\mathcal{G}_\rho(z)$ satisfy the following equation:

$$-\rho z\, e^{-\rho z} = -\rho e^{-\rho}.$$

Thus, the zeros of $\mathcal{G}_\rho(z)$ are

$$z(\rho) := -\frac{1}{\rho} W_k\left(-\rho e^{-\rho}\right), \text{ for } k \in \mathbb{Z}. \tag{1.34}$$

Figure 1.3 depicts the modulus of the zeros $z(\rho)$ for $k \in [-4, 3] \cap \mathbb{Z}$ as a function of the load ρ. The zero having the smallest modulus is given by the principal branch of the Lambert function (drawn in red in Figure 1.3) which is real for any $\rho > 0$ (Note: $-\rho \exp(-\rho)$ is real and $-1/e \leq -\rho \exp(-\rho) < 0$ hence $W_0(-\rho \exp(-\rho))$ is real and negative), thus

$$r_0 = z_0(\rho) = -\frac{1}{\rho} W_0\left(-\rho e^{-\rho}\right)$$

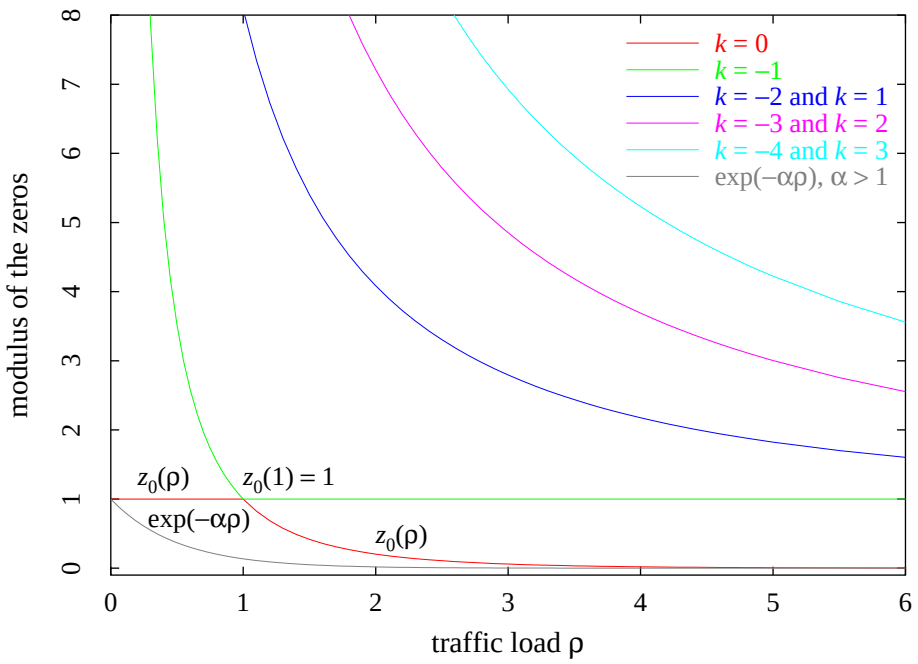

Figure 1.3: Modulus of the zeros of $\mathcal{G}_\rho(z)$, $-\frac{1}{\rho}W_k\left(-\rho e^{-\rho}\right)$, vs. the traffic load ρ

As expected, we find that $z_0(\rho) = 1$ if $\rho \leq 1$; $z_0(\rho) < 1$ if $\rho > 1$; $z_0(1) = 1$ has a multiplicity 2 (because $W_0(-1/e) = W_{-1}(-1/e) = -1$); and for $\rho > 1$, $z_0(\rho)$ is the only zero inside the unit circle. Furthermore, we have that $z_0(\rho)$ is a continuous real function of ρ.

We want to find now a real number r which is smaller than r_0 for any ρ. It can be easily proved that the function $\exp(-\alpha\rho)$ for $\alpha > 1$ serves well, as illustrated in Figure 1.3. Indeed, to have $\exp(-\alpha\rho) < z_0(\rho)$ for $\rho > 0$, it suffices to have $W_0(-\rho\exp(-\rho)) < \rho(\alpha - 1)$. The latter condition is always satisfied for $\alpha > 1$, since $W_0(-\rho\exp(-\rho)) < 0$.

Now that we have found a possible value for the radius of the circle D_r (take $r = \exp(-2\rho)$ for instance), letting $z = r\exp(i\theta) = r\cos\theta + ir\sin\theta$ in (1.32) yields

$$\alpha_j(\rho) = \frac{1}{2\pi r^{j-2}} \int_0^{2\pi} \frac{e^{-i\theta(j-2)}\overline{\mathcal{G}_\rho(\theta)}}{\left|\mathcal{G}_\rho(\theta)\right|^2}\,\mathrm{d}\theta, \tag{1.35}$$

where $\overline{\mathcal{G}_\rho(\theta)}$ denotes the conjugate of $\mathcal{G}_\rho(\theta)$ in the complex plane and $|\mathcal{G}_\rho(\theta)|$ denotes its modulus. We can write:

$$\mathcal{G}_\rho(\theta) = e^{-\rho(1-r\exp(i\theta))} - re^{i\theta}$$
$$\overline{\mathcal{G}_\rho(\theta)} = e^{-\rho(1-r\exp(-i\theta))} - re^{-i\theta}$$
$$\left|\mathcal{G}_\rho(\theta)\right|^2 = r^2 + e^{-2\rho(1-r\cos\theta)} - 2re^{-\rho(1-r\cos\theta)}\cos[\theta - \rho r\sin\theta]$$

$$\begin{aligned} e^{-i\theta(j-2)}\overline{\mathcal{G}_\rho(\theta)} &= e^{-\rho(1-r\cos\theta)}\, e^{-i(\rho r\sin\theta+\theta(j-2))} - re^{-i\theta(j-1)} \\ &= \mathrm{Real}_j(\theta) + i\,\mathrm{Imag}_j(\theta), \end{aligned}$$

where

$$\begin{aligned} \mathrm{Real}_j(\theta) &:= e^{-\rho(1-r\cos\theta)}\cos[\rho r\sin\theta+\theta(j-2)] - r\cos[\theta(j-1)] \\ \mathrm{Imag}_j(\theta) &:= -e^{-\rho(1-r\cos\theta)}\sin[\rho r\sin\theta+\theta(j-2)] + r\sin[\theta(j-1)]. \end{aligned}$$

It is seen that $\mathrm{Real}_j(\theta)$ and $|\mathcal{G}_\rho(\theta)|^2$ are even functions in θ and that $\mathrm{Imag}_j(\theta)$ is odd. Equation (1.35) reduces then to

$$\alpha_j(\rho) = \frac{1}{\pi r^{j-2}}\int_0^\pi \frac{\mathrm{Real}_j(\theta)}{|\mathcal{G}_\rho(\theta)|^2}\mathrm{d}\theta. \tag{1.36}$$

The integral in (1.36) is easily computed using a numerical procedure provided by the NAG[3] C library [91].

1.5.1.2 General remarks

Instead of taking $r = \exp(-\alpha\rho)$ with $\alpha > 1$, it is possible to assign to r any value strictly less than 1 when $\rho \leq 1$ (letting $r = 0.5$ rather than $r = 0.9$ leads to fast convergence when computing numerically the integral). Let us now investigate the case where $\rho > 1$. Notice that $\mathcal{G}_\rho(z)$ has a unique negative real minimum at $1 - \log\rho/\rho$ and that $\mathcal{G}_\rho(0) = \exp(-\rho)$ is positive. Hence, we are sure that r_0 is in the interval $[0, 1 - \log\rho/\rho]$ and may compute r iteratively, starting at $1 - \log\rho/\rho$, and decrementing r until $\mathcal{G}_\rho(r) > 0$.

Since the stationary distribution exists, the coefficients α_j for $j = 2, \ldots, K$ satisfy the following conditions:

- $1 + \rho\,\alpha_K(\rho) > 1$ (existence of π_0),
- $0 < \alpha_2(\rho) - 1 < 1 + \rho\,\alpha_K(\rho)$ (existence of π_1),
- $0 < \alpha_{j+1}(\rho) - \alpha_j(\rho) < 1 + \rho\,\alpha_K(\rho)$ for $j = 2, \ldots, K-1$ (existence of π_j),
- $0 < 1 + (\rho - 1)\alpha_K(\rho) < 1 + \rho\,\alpha_K(\rho)$ (existence of π_K),

which are summarized by:

- $1 < \alpha_2(\rho) < \cdots < \alpha_j(\rho) < \alpha_{j+1}(\rho) < \cdots < \alpha_K(\rho)$ for $j = 2, \ldots, K-1$,
- $\alpha_K(\rho)(1 - \rho) < 1$,

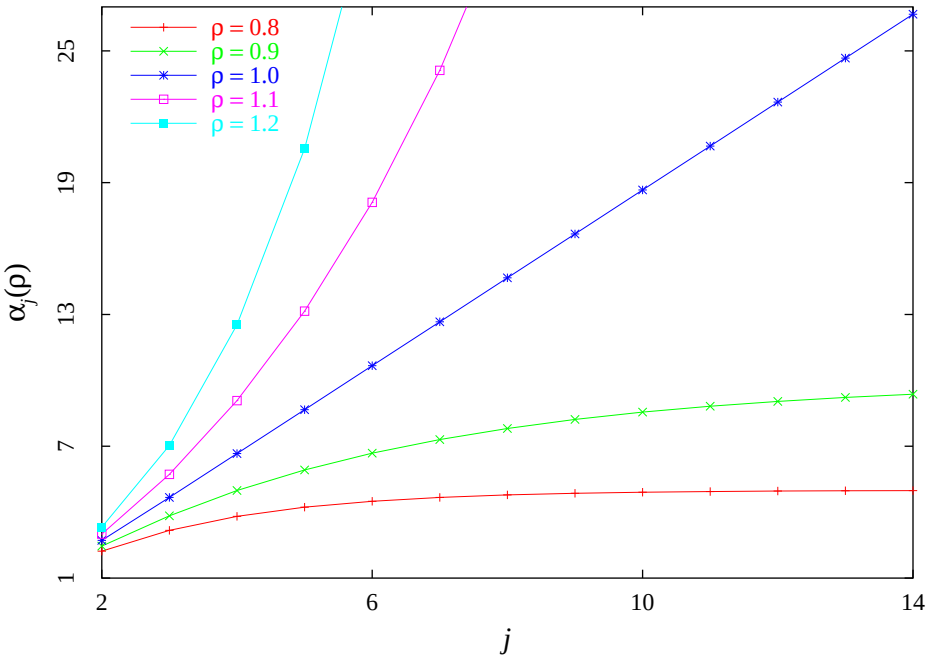

Figure 1.4: The parameter $\alpha_j(\rho)$ for $j = 2, \ldots, K$ and for several values of ρ

- $\alpha_{j+1}(\rho) - \alpha_j(\rho) < 1 + \rho\,\alpha_K(\rho)$ for $j = 2, \ldots, K-2$,

Last, we observe that the function $j \mapsto \alpha_j(\rho)$ is concave increasing for $\rho < 1$, convex increasing for $\rho > 1$ and linear increasing for $\rho = 1$ as plotted in Figure 1.4.

1.5.2 The loss probability

Recall the definition of X_n introduced in Section 1.4.2, $X_n = \mathbf{1}\{Q_n = K\}$ and $X = \lim_{n\to\infty} X_n$. A customer n is lost whenever $X_n = 1$ and is not lost otherwise.

The probability that a foreground customer is lost is the probability that it finds the system full upon arrival, namely,

$$\begin{aligned} P_L &:= P(X = 1) = P(Q = K) \\ &= \frac{1 + (\rho - 1)\,\alpha_K(\rho)}{1 + \rho\,\alpha_K(\rho)}. \end{aligned} \tag{1.37}$$

Notice that in order to have $0 < P_L < 1$, the following condition must be satisfied:

$$0 < \frac{\alpha_K(\rho)}{1 + \rho\,\alpha_K(\rho)} < 1.$$

[3]NAG is a copyright of The Numerical Algorithms Group Ltd

The first inequality says that $\alpha_K(\rho)$ and $1 + \rho\,\alpha_K(\rho)$ must have the same sign. This is always true since both quantities are greater than 1.

The second inequality says that $\alpha_K(\rho) < 1/(1-\rho)$ in the case $\rho < 1$ and $\alpha_K(\rho) > 1/(1-\rho)$ otherwise. The latter is always true, as $\alpha_K(\rho) > 1$ and $1/(1-\rho) < 0$. When $\rho < 1$ and for large values of K, the coefficients α_K become close to each others and very close to $1/(1-\rho)$. A lack of precision during the computation of $\alpha_K(\rho)$ may lead to a negative value for P_L instead of a negligible positive value.

1.5.3 The server utilization

The utilization U of the server was defined as the probability of a non-empty queue. The server utilization is

$$\begin{aligned} U &:= P(Q > 0) \\ &= \frac{\rho\,\alpha_K(\rho)}{1 + \rho\,\alpha_K(\rho)}. \end{aligned} \tag{1.38}$$

Notice that the condition

$$0 < U = \frac{\rho\,\alpha_K(\rho)}{1 + \rho\,\alpha_K(\rho)} < 1$$

is always satisfied.

1.5.4 The expected response time

Applying Little's formula and the PASTA property to the queue, we find that the expected response time R is given by

$$R = \frac{\sum_{j=1}^{K} j\,\pi(j)}{(\lambda+\gamma)(1-\pi_K)}. \tag{1.39}$$

Using (1.29), (1.30) and (1.31), (1.39) rewrites

$$R = \frac{K(1+\rho\alpha_K(\rho)) - \left[1 + \sum_{j=2}^{K} \alpha_j(\rho)\right]}{\mu\,\rho\,\alpha_K(\rho)} \tag{1.40}$$

with $\alpha_j(\rho)$ defined in (1.32).

1.6 Using the inference models

1.6.1 An inference question

Until now we have introduced two models for a connection. In the first model, we were able to identify five metrics describing the quality of service provided to the foreground source, P_L, U, R, q_L and q_N, given in (1.3), (1.5), (1.10), (1.18) and (1.21). In the second model, we were able to identify three QoS metrics, P_L, U and R, given in (1.37), (1.38) and (1.40). Since $\rho = (\lambda + \gamma)/\mu$, all these equations are expressed in terms of the parameters λ, μ and K (the probing rate γ is known).

The problem is therefore the following: How can we infer estimates $\hat{\lambda}_n$, $\hat{\mu}_n$ and $\hat{K}_n$ of parameters λ, μ and K, respectively, from the observations collected from the first n probes?

If the parameters λ, μ and K are unknown, then (1.3), (1.5), (1.10), (1.18) and (1.21) leave us with nine schemes to compute these three constants in the $M/M/1/K$ case (there are $C_5^3 = 10$ possible schemes but relation (1.22) reduces that number to nine); only one scheme is available in the $M/D/1/K$ case. These ten schemes are listed in Table 1.1, where the notation X_Y_Z denotes the scheme obtained by using the metrics X, Y and Z in the $M/M/1/K$ case and where $P_L\_U\_R\_D$ denotes the scheme obtained by using the metrics P_L, U and R in the $M/D/1/K$ case.

Table 1.1: Schemes for estimating λ, μ and K

Scheme	Reference	Equations to use
$P_L\_U\_R$	*1*	(1.3), (1.5), (1.10)
$P_L\_U\_q_L$	*2*	(1.3), (1.5), (1.18)
$P_L\_U\_q_N$	*3*	(1.3), (1.5), (1.21)
$P_L\_R\_q_L$	*4*	(1.3), (1.10), (1.18)
$P_L\_R\_q_N$	*5*	(1.3), (1.10), (1.21)
$U\_R\_q_L$	*6*	(1.5), (1.10), (1.18)
$U\_R\_q_N$	*7*	(1.5), (1.10), (1.21)
$U\_q_L\_q_N$	*8*	(1.5), (1.18), (1.21)
$R\_q_L\_q_N$	*9*	(1.10), (1.18), (1.21)
$P_L\_U\_R\_D$	*10*	(1.37), (1.38), (1.40)

If we now assume that only λ and K are unknown (μ being estimated for instance, using *pathrate* [46], PBM [94] or ROPP [77], see Section 1.2), then $C_5^2 = 10$ schemes in the $M/M/1/K$ case and one scheme in the $M/D/1/K$ case (Equation (1.40) can be used only if (1.37)–(1.38) are also used) can be used to compute these two constants, resulting in a total of eleven schemes. These eleven schemes are listed in Table 1.2, where the notation X_Y denotes the scheme obtained by using the metrics X and Y in the $M/M/1/K$ case

and where $P_L\_U\_D$ denotes the scheme obtained by using the metrics P_L and U in the $M/D/1/K$ case.

Table 1.2: Schemes for estimating λ and K (μ assumed to be already known/estimated)

Scheme	Reference	Equations to use
P_L_U	**I**	(1.3), (1.5)
P_L_R	**II**	(1.3), (1.10)
$P_L\_q_L$	**III**	(1.3), (1.18)
$P_L\_q_N$	**IV**	(1.3), (1.21)
U_R	**V**	(1.5), (1.10)
U_q_L	**VI**	(1.5), (1.18)
U_q_N	**VII**	(1.5), (1.21)
R_q_L	**VIII**	(1.10), (1.18)
R_q_N	**IX**	(1.10), (1.21)
$q_L\_q_N$	**X**	(1.18), (1.21)
$P_L\_U\_D$	**XI**	(1.37), (1.38)

1.6.2 Solving for the equations

Up to now, we have defined two groups of schemes. The schemes, denoted by the italic numbers *1*,...,*10*, have three QoS metrics as inputs and can be used to simultaneously estimate parameters λ, μ and K. The schemes, denoted by the roman numbers **I**,...,**XI**, have two QoS metrics as inputs and can be used to estimate parameters λ and K solely, parameter μ being known/estimated beforehand by using some other technique (the *pathrate* tool for instance). Assume that the QoS metrics involved in a scheme can be evaluated from measurements collected at the sender/receiver (cf. Section 1.6.3). Then, estimators for λ, μ and K (or for λ and K only) are obtained by "solving" the scheme with respect to (w.r.t.) the variables λ, μ and K (or w.r.t. the variables λ and K).

If we want to apply a certain scheme to estimate the buffer size, the intensity of the cross traffic, and possibly the server capacity, we must establish existence and uniqueness of its solution (λ, μ, K) or (λ, K). To be more precise, consider for instance scheme **I** that involves the loss probability P_L and the server utilization U (μ is known). Then, for any (measured) values of P_L and U with $0 < P_L < 1$ and $0 < U < 1$, we want to find a single pair (λ, K) satisfying the set of equations defined by (1.3) and (1.5). This existence and uniqueness property holds for scheme *1*, as shown below, as well as for schemes *10*, **I**, **II**, **V** and **XI**. As for the other schemes we have not been able to show that property, but in all experiments that have been carried out, and that are reported in Section 1.7, each scheme always gave us a unique solution. We now discuss the solution to scheme *1*, and indicate how the solution of scheme *10* can be derived. We next discuss the solution to scheme **I**,

show the existence and uniqueness of the solution for schemes **II** and **V**, and indicate how the solution of scheme **XI** can be found.

1.6.2.1 Solving for scheme *1*

The equations involved here are (1.3), (1.5) and (1.10), namely,

$$P_L = \frac{(1-\rho)\,\rho^K}{1-\rho^{K+1}},$$

$$U = \rho\left(\frac{1-\rho^K}{1-\rho^{K+1}}\right) = \rho\,(1-P_L),$$

$$R = \frac{1}{\mu\,(1-\rho)} - \frac{K}{\mu}\,\frac{\rho^K}{1-\rho^K} = \frac{1}{\mu\,(1-\rho)}\left(1 - \frac{K\,P_L}{1-P_L}\right).$$

These equations produce the following expressions to ρ and μ,

$$\rho = \frac{U}{1-P_L} \qquad \text{i.e.} \qquad \lambda = \frac{\mu\,U}{1-P_L} - \gamma \tag{1.41}$$

$$\mu = \frac{1}{R\,(1-\rho)}\left(1 - \frac{K\,P_L}{1-P_L}\right) = \frac{1-P_L(K+1)}{R\,(1-P_L-U)}. \tag{1.42}$$

Combining (1.41) and (1.7) yields an additional expression to K,

$$K = \frac{\log(P_L/(1-U))}{\log(U/(1-P_L))}. \tag{1.43}$$

1.6.2.2 Solving for scheme *10*

This scheme still involves P_L, U and R, but this time these quantities have to be computed for the $M{+}M/D/1/K$ queue. More precisely, cf. (1.37), (1.38) and (1.40),

$$P_L = \frac{1+(\rho-1)\,\alpha_K(\rho)}{1+\rho\,\alpha_K(\rho)}, \tag{1.44}$$

$$U = \frac{\rho\,\alpha_K(\rho)}{1+\rho\,\alpha_K(\rho)}, \tag{1.45}$$

$$R = \frac{K(1+\rho\alpha_K(\rho)) - \left[1+\sum_{j=2}^{K}\alpha_j(\rho)\right]}{\mu\,\rho\,\alpha_K(\rho)} \tag{1.46}$$

with $\alpha_K(\rho)$ given in (1.32).

Recall that we want to solve the system of equations (1.44)–(1.46) with respect to the variables λ, μ and K. We readily observe from (1.44)–(1.46) that

$$\rho = \frac{U}{1-P_L} \qquad \text{i.e.} \qquad \lambda = \frac{\mu U}{1-P_L} - \gamma, \tag{1.47}$$

$$\alpha_K(\rho) = \frac{1-P_L}{1-U}, \tag{1.48}$$

$$\mu = \frac{K - (1-U)\left[1 + \sum_{j=2}^{K} \alpha_j(\rho)\right]}{RU}. \tag{1.49}$$

Since all coefficients $\{\alpha_j(\rho), j \geq 2\}$ in the Taylor series expansion of $1/\mathcal{G}_\rho(z)$ are different (see Section 1.5.1.2), then (1.47)–(1.48) returns a unique solution (ρ, K).

For a given ρ, we computed the coefficients $\alpha_j(\rho)$ for a certain range of j and compared the results with the r.h.s. of (1.48); then K was chosen as the integer j for which $\alpha_j(\rho)$ was the closest to (the measured value of) $(1-P_L)/(1-U)$.

Having K at our disposal, as well as the coefficients $\{\alpha_j(\rho), 2 \leq j \leq K\}$, it is then possible to infer μ using (1.49), and subsequently λ using (1.47).

1.6.2.3 Solving for scheme I

The equations involved here are (1.3) and (1.5), namely,

$$P_L = \frac{(1-\rho)\,\rho^K}{1-\rho^{K+1}},$$

$$U = \rho\left(\frac{1-\rho^K}{1-\rho^{K+1}}\right) = \rho\,(1-P_L).$$

These yield the following expressions to ρ and K,

$$\rho = \frac{U}{1-P_L}, \quad \text{i.e.} \quad \lambda = \frac{\mu U}{1-P_L} - \gamma, \tag{1.50}$$

$$K = \frac{\log(P_L/(1-U))}{\log(U/(1-P_L))}, \tag{1.51}$$

where the last equation is obtained by combining (1.50) and (1.7). Therefore, the set of equations (1.3) and (1.5) in the variables λ and K has a unique solution given in (1.50) and (1.51), respectively.

It is interesting to investigate the sensitivity of λ and K with respect to the variables P_L and U. To do so, let us compute the differentials of λ and K considered as functions of

P_L and U. From (1.50) and (1.51) we find

$$\mathrm{d}\lambda = \frac{\mu}{1-P_L}\left(\mathrm{d}U + \frac{U}{1-P_L}\,\mathrm{d}P_L\right),$$
$$\mathrm{d}K = \frac{1}{\log^2(U/(1-P_L))}\Big(A\,\mathrm{d}U + B\,\mathrm{d}P_L\Big),$$

where

$$A = \frac{\log(U/(1-P_L))}{1-U} - \frac{\log(P_L/(1-U))}{U},$$
$$B = \frac{\log(U/(1-P_L))}{P_L} - \frac{\log(P_L/(1-U))}{1-P_L}.$$

Using (1.3) and (1.5), A and B are rewritten as follows:

$$A = \frac{\log\rho(1-\rho^{K+1})}{\rho^K(1-\rho)(1-\rho^K)}\Big(\rho^K(1-\rho^K) - K\rho^{K-1}(1-\rho)\Big),$$
$$B = \frac{\log\rho(1-\rho^{K+1})}{\rho^K(1-\rho)(1-\rho^K)}\Big(1-\rho^K - K\rho^K(1-\rho)\Big).$$

We find that $A > 0$ and $B < 0$ for any value of ρ. Comparing $|A|$ and $|B| = -B$, we obtain $|A| > |B|$ for $\rho > 1$ and $|A| < |B|$ for $\rho < 1$. We deduce that K follows primarily U's variations for $\rho > 1$ (since $|A| > |B|$) and it is more influenced by P_L's variations than by U's variations for $\rho < 1$ (since $|A| < |B|$). As for λ, it is more sensitive to the variations of P_L (resp. U) than to the variations of U (resp. P_L) whenever $\rho = U/(1-P_L) > 1$ (resp. $\rho < 1$). When $\rho = 1$ ($U = 1 - P_L$), both λ and K are equally influenced by P_L and U's variations since in this case

$$\mathrm{d}\lambda = \frac{\mu}{1-P_L}\Big(\mathrm{d}U + \mathrm{d}P_L\Big),$$
$$\mathrm{d}K = \frac{1}{2}\,(K+1)^2(\mathrm{d}U - \mathrm{d}P_L).$$

In other words, when $\rho > 1$ (resp. $\rho < 1$), fast convergence in the estimation of P_L (resp. of U) leads to fast convergence in the estimation of λ while slow convergence in the estimation of U (resp. of P_L) leads to slow convergence in the estimation of K.

1.6.2.4 Solving for scheme II

Assume that one knows R and P_L and that ρ and K are unknown. The expression

for P_L (1.3) yields the following expression for K in terms of ρ and P_L,

$$K = \frac{\log(P_L/(1-\rho\,(1-P_L)))}{\log\rho}. \tag{1.52}$$

Substituting this value of K into (1.9) yields

$$R = \frac{1}{\mu\,(1-\rho)} - \frac{P_L\,\log(P_L/(1-\rho\,(1-P_L)))}{\mu\,(1-\rho)\,(1-P_L)\,\log\rho}.$$

Observe that necessarily $\rho < 1/(1-P_L)$. For $0 < x < 1/(1-P_L)$, we introduce the mapping

$$f(x) := \frac{1}{\mu\,(1-x)} - \frac{P_L\,\log(P_L/(1-x\,(1-P_L)))}{\mu\,(1-x)\,(1-P_L)\,\log x} - R. \tag{1.53}$$

If one can show that the equation $f(x) = 0$ has a unique solution in $(0, 1/(1-P_L))$, then this solution yields ρ, hence λ, and subsequently K by using (1.52). Proposition 1.6.1 shows that this is indeed the case.

Proposition 1.6.1 *For any constants $\mu > 0$, $P_L \in (0,1)$ and $R \geq 1/\mu$, the equation $f(x) = 0$ has a unique solution in $[0, 1/(1-P_L)]$.* ♦

Proof. Define

$$g(x) := (1-P_L)\,(1-R\mu\,(1-x))\log x - P_L\,\log P_L + P_L\,\log(1-x\,(1-P_L)) \tag{1.54}$$

for $0 < x < 1/(1-P_L))$. Hence, cf. (1.53),

$$f(x) := \frac{g(x)}{\mu\,(1-P_L)(1-x)\log x}. \tag{1.55}$$

Denote by $g^{(1)}(x)$ (resp. $g^{(2)}(x)$) the first (resp. second) order derivative of $g(x)$. We find

$$g^{(1)}(x) = (1-P_L)\,R\mu\left(\log x - \frac{(1-P_L)(x-1)(x+a)}{x\,(1-x(1-P_L))}\right) \tag{1.56}$$

with

$$a := \frac{R\mu - 1}{R\mu\,(1-P_L)} \geq 0, \tag{1.57}$$

and

$$g^{(2)}(x) = \frac{(1-P_L)R\mu\,h(x)}{x^2\,(1-x(1-P_L))^2} \tag{1.58}$$

with

$$\begin{aligned} h(x) \;:=\; & (1-P_L)^2\,x^3 + ((1+a)\,P_L^2 + (1-2a)\,P_L - (2-a))x^2 \\ & + (1-2a\,(1-P_L)^2)\,x + a(1-P_L). \end{aligned} \tag{1.59}$$

From the identities

$$g(1) = 0, \qquad g^{(1)}(1) = 0 \qquad \text{and} \qquad g^{(2)}(1) = \left(\frac{1-P_L}{P_L}\right)(2R\mu P_L - 1)$$

we see, by applying l'Hôpital's rule to the r.h.s. of (1.55), that $f(1)$ is well-defined, with value

$$f(1) = -\frac{g^{(2)}(1)}{2\mu(1-P_L)} = -\frac{2R\mu P_L - 1}{2\mu P_L}. \tag{1.60}$$

Therefore, unless $g^{(2)}(1) = 0$, the zeros of $f(x)$ in $(0, 1/(1-P_L))$ are the zeros of $g(x)$ in $(0, 1/(1-P_L)) \setminus \{1\}$; if $g^{(2)}(1) = 0$, then $f(x)$ and $g(x)$ have the same zeros in $(0, 1/(1-P_L))$.

We now show that $g(x)$ has a unique zero in $(0, 1/(1-P_L)) \setminus \{1\}$ when $g^{(2)}(1) \neq 0$ and that $g(x)$ has a unique zero in $(0, 1/(1-P_L))$, located at the point $x = 1$, when $g^{(2)}(1) = 0$, which will conclude the proof.

Assume first that $a \neq 0$. It is then seen from the identities

$$\begin{array}{ll} h(0) = a\,(1-P_L) > 0, & \lim_{x\to-\infty} h(x) = -\infty, \\ h(1/(1-P_L)) = -\frac{1}{(1-P_L)R\mu} < 0, & \lim_{x\to+\infty} h(x) = +\infty, \end{array} \tag{1.61}$$

that the polynomial $h(x)$ of degree 3 in the variable x has exactly one root $x = \rho(a)$ in $(0, 1/(1-P_L))$. Combining (1.61) and (1.58) yields

$$\begin{array}{ll} g^{(2)}(x) > 0, \text{ for } 0 < x < \rho(a), & \lim_{x\to 0} g^{(2)}(x) = \infty, \\ g^{(2)}(x) < 0, \text{ for } \rho(a) < x < 1/(1-P_L), & \lim_{x\to 1/(1-P_L)} g^{(2)}(x) = -\infty, \\ g^{(2)}(\rho(a)) = 0. & \end{array}$$

Assume now that $a = 0$. Then, cf. (1.58)–(1.59),

$$g^{(2)}(x) = \frac{(1-P_L)\,R\mu}{x\,(1-x(1-P_L))^2}\,k(x) \tag{1.62}$$

with

$$k(x) := (1-P_L)^2\,x^2 + (P_L^2 + P_L - 2)x + 1. \tag{1.63}$$

From

$$k(0) = 1, \qquad k(1/(1-P_L)) = -P_L, \qquad \text{and} \qquad \lim_{x\to\infty} k(x) = \infty,$$

we deduce that the polynomial $k(x)$, of degree 2 in the variable x, has exactly one zero, $x = \rho(0)$, in $(0, 1/(1-P_L))$. This in turn implies from (1.62) that

$$\begin{array}{ll} g^{(2)}(x) > 0, \text{ for } 0 < x < \rho(0), & \lim_{x\to 0} g^{(2)}(x) = \infty, \\ g^{(2)}(x) < 0, \text{ for } \rho(0) < x < 1/(1-P_L), & \lim_{x\to 1/(1-P_L)} g^{(2)}(x) = -\infty, \\ g^{(2)}(\rho(0)) = 0, & \end{array}$$

In summary, we have shown that for all $a \geq 0$, $g^{(2)}(x)$ has a unique zero $x = \rho(a)$ in $(0, 1/(1-P_L))$; furthermore, $g^{(2)}(x) > 0$ for $0 < x < \rho(a)$ and $g^{(2)}(x) < 0$ for $\rho(a) < x < 1/(1-P_L))$.

From the above we may now determine the variations of the function $g(x)$ in $(0, 1/(1-P_L))$. This is done in Figures (1.5)–(1.7) by distinguishing the cases when (i) $0 < \rho(a) < 1$, (ii) $1 < \rho(a) < 1/(1-P_L)$ and (iii) $\rho(a) = 1$.

- $0 < \rho(a) < 1$

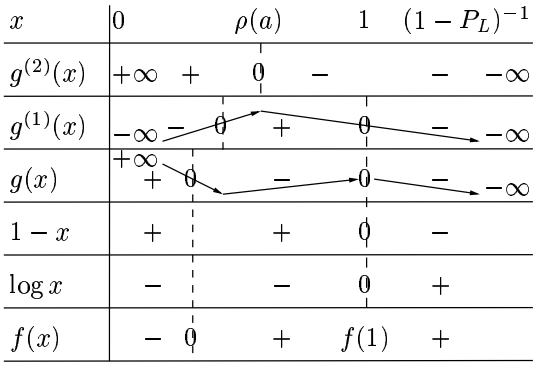

Figure 1.5: $0 < \rho(a) < 1$

We conclude from Figure 1.5 that $g(x)$ has a unique zero in $(0, 1/(1-P_L)) \setminus \{1\}$ when $0 < \rho(a) < 1$. This zero is located in $(0, \rho(a))$

- $1 < \rho(a) < 1/(1-P_L)$

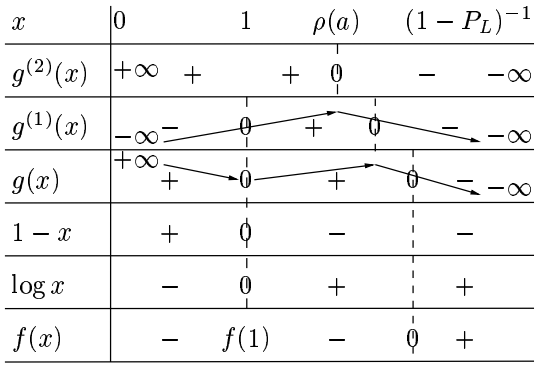

Figure 1.6: $1 < \rho(a) < 1/(1 - P_L)$

We conclude from Figure 1.6 that $g(x)$ has a unique zero in $(0, 1/(1-P_L)) \setminus \{1\}$ when $0 < \rho(a) < 1$. This zero is located in $(\rho(a), 1/(1-P_L))$.

- $\rho(a) = 1$

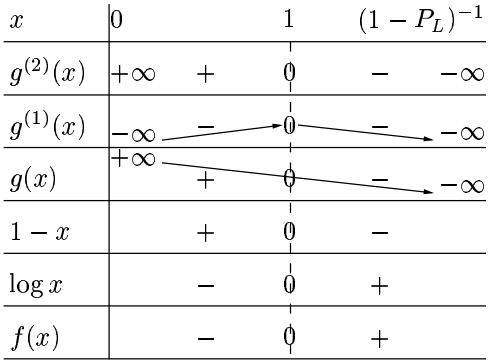

Figure 1.7: $\rho(a) = 1$

In this case, $x = 1$ in the only zero of $g(x)$ in $(0, 1/(1-P_L))$ (cf. Figure 1.7). This is a zero of multiplicity 3.

■

It is interesting to investigate the sensitivity of λ and K with respect to the variables R and P_L. To do so, let us compute the differentials of λ and K considered as functions of R and P_L. From (1.10) and (1.3) we have

$$\mathrm{d}R = C\,\mathrm{d}\lambda + D\,\mathrm{d}K \tag{1.64}$$

$$\mathrm{d}P_L = E\,\mathrm{d}\lambda + F\,\mathrm{d}K \tag{1.65}$$

with

$$C = \frac{\partial R}{\partial \rho}\frac{\partial \rho}{\partial \lambda} = \frac{1}{\mu^2(1-\rho)^2} - \frac{K^2\rho^{K-1}}{\mu^2(1-\rho^K)^2},$$
$$D = \frac{\partial R}{\partial K} = -\frac{\rho^K(1+K\log\rho-\rho^K)}{\mu(1-\rho^K)^2},$$
$$E = \frac{\partial P_L}{\partial \rho}\frac{\partial \rho}{\partial \lambda} = \frac{\rho^{K-1}(K(1-\rho)-\rho(1-\rho^K))}{\mu(1-\rho^{K+1})^2},$$
$$F = \frac{\partial P_L}{\partial K} = \frac{\rho^K(1-\rho)\log\rho}{(1-\rho^{K+1})^2}.$$

From (1.64) and (1.65), we can write

$$d\lambda = \frac{F}{CF-DE}\mathrm{d}R - \frac{D}{CF-DE}\mathrm{d}P_L$$
$$dK = -\frac{E}{CF-DE}\mathrm{d}R + \frac{C}{CF-DE}\mathrm{d}P_L.$$

It is seen that $C \geq 0$, $D > 0$, $E > 0$ and $F < 0$ for any $\rho > 0$ and any $K \geq 1$. To identify which parameter affects the most λ (resp. K), one should compare $-F$ to D (resp. E to C). Unfortunately the sign of $D+F$ (resp. $C-E$) depends on the values of μ, ρ and K, and it is impossible to formally identify which estimator among R and P_L has the biggest impact on the estimation of λ and K.

1.6.2.5 Solving for scheme V

Scheme **V** involves Equations (1.5) and (1.10)

$$U = \rho\left(\frac{1-\rho^K}{1-\rho^{K+1}}\right)$$
$$R = \frac{1}{\mu\,(1-\rho)} - \frac{K}{\mu}\,\frac{\rho^K}{1-\rho^K}. \tag{1.66}$$

The expression for R in (1.9) is useful here

$$R = \frac{1}{\mu\,(1-\rho)} - \frac{K}{\mu}\,\frac{\pi_K}{(1-\rho)\,(1-\pi_K)}. \tag{1.67}$$

Using (1.6), π_K can be expressed as

$$\pi_K = 1 - U/\rho, \tag{1.68}$$

to yield from (1.67)

$$R = \frac{1}{\mu\,(1-\rho)} - \frac{K}{\mu}\,\frac{\rho - U}{(1-\rho)\,U}. \tag{1.69}$$

Recall the relation (1.7) for K

$$K = \frac{1}{\log \rho} \cdot \log\left(\frac{1 - U/\rho}{1-U}\right).$$

Substituting Equation (1.7) for K into (1.69) yields

$$R = \frac{1}{\mu\,(1-\rho)} - \frac{\rho - U}{\mu U\,(1-\rho)\,\log \rho}\,\log\left(\frac{\rho - U}{\rho\,(1-U)}\right). \tag{1.70}$$

Observe that necessarily $\rho \geq U$. For $\rho \geq U$, introduce the mapping

$$f(x) = \frac{1}{\mu\,(1-x)} - \frac{x - U}{\mu U\,(1-x)\,\log x}\,\log\left(\frac{x - U}{x\,(1-U)}\right) - R. \tag{1.71}$$

If one can show that the equation $f(x) = 0$ has a unique solution in $[U, \infty)$, then this solution yields ρ, and subsequently K by using (1.7). Proposition 1.6.2 shows that this is indeed the case.

Proposition 1.6.2 *For any constants μ, U and R such that $\mu > 0$, $0 < U < 1$ and $R \geq 1/\mu$, the equation $f(x) = 0$ has a unique solution in $[U, \infty)$.* ♦

Proof. Define

$$g(x) = U\,\log x - (x - U)\,\log\left(\frac{x - U}{x\,(1-U)}\right) - \mu R U\,(1-x)\,\log x$$

for $x \geq U$. Hence (1.71) rewrites as

$$f(x) = \frac{g(x)}{\mu U\,(1-x)\,\log x}. \tag{1.72}$$

Denote by $g^{(1)}(x)$ (resp. $g^{(2)}(x)$) the first (resp. second) order derivative of $g(x)$. We find

$$g^{(1)}(x) = \mu R U\,\log x - \mu R U\,\frac{1-x}{x} - \log\left(\frac{x - U}{x\,(1-U)}\right) \tag{1.73}$$

and

$$\begin{aligned} g^{(2)}(x) &= \frac{\mu R U}{x} + \frac{\mu R U}{x^2} - \frac{U}{x\,(x-U)} \\ &= \frac{U\,h(x)}{x^2\,(x-U)} \end{aligned} \tag{1.74}$$

with

$$h(x) := \mu R x^2 - [1 - \mu R(1-U)]\, x - \mu R U. \tag{1.75}$$

The function $h(x)$ has two zeros

$$x_1 = \frac{1 - \mu R(1-U) - \sqrt{[1-\mu R(1-U)]^2 + 4\mu^2 R^2 U}}{2\mu R}$$
$$x_2 = \frac{1 - \mu R(1-U) + \sqrt{[1-\mu R(1-U)]^2 + 4\mu^2 R^2 U}}{2\mu R}.$$

It is clear that $x_1 \leq 0$. As for x_2, observe that $h(U) = -U \leq 0$. Since $h(x_2) = 0$ and $\lim_{x\to\pm\infty} h(x) = +\infty$, it follows that $x_2 \geq U$. Hence $h(x)$ has only one zero in $[U, \infty)$.

Looking at expression (1.72), we can say that, unless $x = 1$, the zeros of $g(x)$ are the zeros of $f(x)$. For $x = 1$, we have $g(1) = 0$, $g^{(1)}(1) = 0$ and $g^{(2)}(1) = 2\mu RU - U/(1-U)$. By applying l'Hôpital's rule to the right-hand side of (1.72), we see that $f(1)$ is well-defined, with value

$$\begin{aligned} f(1) &= \frac{g^{(2)}(1)}{-2\mu U} \\ &= \frac{1 - 2\mu R\,(1-U)}{2\mu\,(1-U)}. \end{aligned} \tag{1.76}$$

$f(1) = 0$ if and only if $g^{(2)}(1) = 0$ i.e. if $1 - 2\mu R\,(1-U) = 0$. Therefore, unless this condition is satisfied, the zeros of $f(x)$ in $[U, \infty)$ are the zeros of $g(x)$ in $[U, \infty) \setminus \{1\}$; for $1 - 2\mu R\,(1-U) = 0$, the zeros of $f(x)$ in $[U, \infty)$ are the zeros of $g(x)$ in $[U, \infty)$. In that case, (1.75) rewrites as

$$h(x) = \mu\, R\,(x^2 - (1-U)x - U)$$

and its zeros become $x_1 = -U$ and $x_2 = 1$.

Three cases are to be considered depending on whether x_2 is less than, equal to or greater than 1 (we have seen that $x_2 = 1$ if $1 - 2\mu R(1-U) = 0$). In each case, the variations of the functions $g(x)$ and $f(x)$ are studied. We aim at showing that $g(x)$ has a unique zero in $[U, \infty) \setminus \{1\}$ when $g^{(2)}(1) \neq 0$ and a unique zero in $[U, \infty)$, located at the point $x = 1$, when $g^{(2)}(1) = 0$, which will conclude the proof. The following limits are easily calculated

$$\lim_{x\to+\infty} g^{(2)}(x) = 0, \qquad \lim_{x\to\pm\infty} g^{(1)}(x) = +\infty,$$
$$\lim_{x\to-\infty} g^{(2)}(x) = -\infty, \qquad \lim_{x\to+\infty} g(x) = +\infty.$$

- $U \leq x_2 \leq 1$

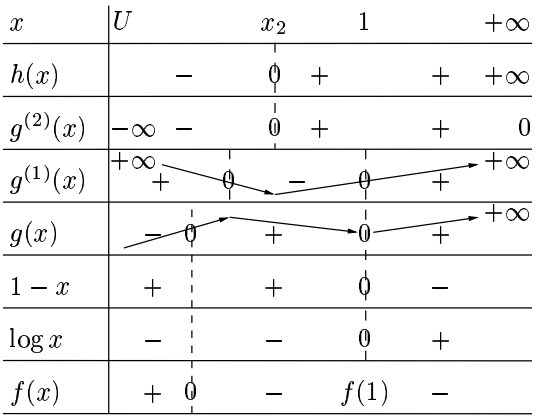

Figure 1.8: $U \leq x_2 \leq 1$

We conclude from Figure 1.8 that $g(x)$ has a unique zero in $[U, \infty) \setminus \{1\}$ when $U \leq x_2 \leq 1$. This zero is located in $[U, x_2)$

- $x_2 \geq 1$

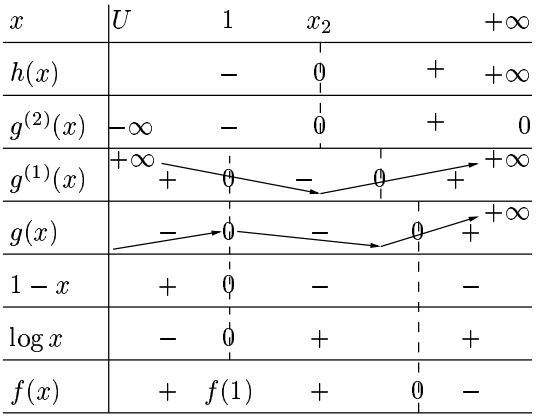

Figure 1.9: $x_2 \geq 1$

We conclude from Figure 1.9 that $g(x)$ has a unique zero in $[U, \infty) \setminus \{1\}$ when $x_2 \geq 1$. This zero is located in (x_2, ∞)

- $x_2 = 1$ (i.e. $1 - 2\mu R\,(1 - U) = 0$)

x	U		$x_2 = 1$		$+\infty$
$h(x)$		$-$	0	$+$	$+\infty$
$g^{(2)}(x)$	$-\infty$	$-$	0	$+$	0
$g^{(1)}(x)$	$+\infty$	$+$	0	$+$	$+\infty$
$g(x)$		$-$	0	$+$	$+\infty$
$1-x$		$+$	0	$-$	
$\log x$		$-$	0	$+$	
$f(x)$		$+$	0	$-$	

Figure 1.10: $x_2 = 1$

In this case (cf. Figure 1.10), $g(x)$ has only one zero in $[U, \infty)$ which is $x_2 = 1$.

■

Concerning the sensitivity of λ and K with respect to the variables U and R, a similar analysis as the one in Section 1.6.2.4 can be performed, leading to the same conclusion: $\mathrm{d}\lambda$ and $\mathrm{d}K$ depend on the values of μ, ρ and K and it is rather impossible to formally identify which estimator among U and R has the biggest impact on the estimations of λ and K.

1.6.2.6 Solving for scheme XI

This scheme has P_L and U as inputs, but this time these quantities have to be computed for the $M{+}M/D/1/K$ queue. More precisely, cf. (1.37) and (1.38),

$$P_L = \frac{1 + (\rho - 1)\,\alpha_K(\rho)}{1 + \rho\,\alpha_K(\rho)} \tag{1.77}$$

$$U = \frac{\rho\,\alpha_K(\rho)}{1 + \rho\,\alpha_K(\rho)} \tag{1.78}$$

with $\alpha_K(\rho)$ given in (1.33).

Recall that we want to solve the system of equations (1.77)–(1.78) with respect to the variables λ and K. We readily observe from (1.77)–(1.78) that

$$\rho = \frac{U}{1 - P_L}, \quad \text{i.e.} \quad \lambda = \frac{\mu\,U}{1 - P_L} - \gamma \tag{1.79}$$

$$\alpha_K(\rho) = \frac{1 - P_L}{1 - U}. \tag{1.80}$$

Since all coefficients $\{\alpha_j(\rho), j \geq 2\}$ in the Taylor series expansion of $1/\mathcal{G}_\rho(z)$ are different (see Section 1.5.1.2), then (1.79)–(1.80) will return a unique solution (ρ, K).

For a given ρ, we computed the coefficients $\alpha_j(\rho)$ for a certain range of values for j and compared the results with the r.h.s. of (1.80); then K was chosen as the integer j for which $\alpha_j(\rho)$ was the closest to (the measured value of) $(1 - P_L)/(1 - U)$.

1.6.3 Calculating the moment-based estimators

We have at our disposal the first n samples of $\{X_i\}_i$, $\{Y_i\}_i$, $\{a_i\}_i$, $\{d_i\}_i$ for the probing traffic, and we know γ and μ. Let $\hat{U}(n)$, $\hat{P}_L(n)$, $\hat{R}(n)$, $\hat{q}_L(n)$ and $\hat{q}_N(n)$ denote the estimators of U, P_L, R, q_L and q_N, respectively. They are defined as $(n = 1, 2, \ldots)$

$$\hat{P}_L(n) := \frac{1}{n} \sum_{i=1}^{n} \mathbf{1}\{X_i = 1\}, \tag{1.81}$$

$$\hat{U}(n) := \frac{1}{n} \sum_{i=1}^{n} \mathbf{1}\{Y_i = 1\}, \tag{1.82}$$

$$\hat{R}(n) := \frac{\sum_{i=1}^{n} \mathbf{1}\{X_i = 0\}\,(d_i - a_i)}{\sum_{i=1}^{n} \mathbf{1}\{X_i = 0\}}, \text{ for } \sum_{i=1}^{n} \mathbf{1}\{X_i = 0\} > 0, \tag{1.83}$$

$$\hat{q}_L(n) := \frac{\sum_{i=1}^{n-1} \mathbf{1}\{X_i = 1, X_{i+1} = 1\}}{\sum_{i=1}^{n-1} \mathbf{1}\{X_i = 1\}}, \text{ for } \sum_{i=1}^{n-1} \mathbf{1}\{X_i = 1\} > 0, \tag{1.84}$$

$$\hat{q}_N(n) := \frac{\sum_{i=1}^{n-1} \mathbf{1}\{X_i = 0, X_{i+1} = 0\}}{\sum_{i=1}^{n-1} \mathbf{1}\{X_i = 0\}}, \text{ for } \sum_{i=1}^{n-1} \mathbf{1}\{X_i = 0\} > 0. \tag{1.85}$$

The estimates $\hat{P}_L(n)$ and $\hat{U}(n)$ are obtained using all observations, $\hat{R}(n)$ and $\hat{q}_N(n)$ are obtained using observations corresponding to successful packets, and $\hat{q}_L(n)$ is obtained using observations corresponding to lost packets. We expect $\hat{q}_L(n)$ to converge slowly to q_L, hence, intuitively, we can say that all schemes involving this metric will not perform well.

1.6.4 Desirable properties of an estimator

If a comparison is to be made among several estimators, it is useful to identify the main properties expected of a good estimator. Namely, an estimator is preferably unbiased and consistent. Unbiasedness has been proven for $\hat{P}_L(n)$, $\hat{U}(n)$ and $\hat{R}(n)$, while $\hat{q}_L(n)$ and $\hat{q}_N(n)$ turn out to be biased (see next Section). Consistency[4] for each metric is much more complicated to show. Establishing such a property implies computing both the bias and the

[4] A consistent estimator is one that concentrates completely on its target as the sample size increases

variance of an estimator. The major difficulty in this computation is due to the fact that the random variables $\{X_i\}_i$ are correlated, since the queue is finite and since the samples are taken from consecutive foreground packets, rather than random packets.

1.6.4.1 Study of the mean values

Using the identity $\mathbf{E}[\mathbf{1}\{A\}] = P(A)$ that holds for any event A, we find

$$\mathbf{E}[\hat{P}_L(n)] = P_L,$$
$$\mathbf{E}[\hat{U}(n)] = U,$$
$$\mathbf{E}[\hat{R}(n)] = R,$$
$$\mathbf{E}[\hat{q}_L(n)] = q_L - \frac{\mathrm{cov}[\hat{q}_L(n), \hat{P}_L(n-1)]}{P_L},$$
$$\mathbf{E}[\hat{q}_N(n)] = q_N + \frac{\mathrm{cov}[\hat{q}_N(n), \hat{P}_L(n-1)]}{P_L}.$$

The last two equalities follow from (1.84) and (1.85) when expressed as follows

$$\hat{q}_L(n) = \frac{\sum_{i=1}^{n-1} \mathbf{1}\{X_i = 1, X_{i+1} = 1\}}{(n-1)\,\hat{P}_L(n-1)},$$
$$\hat{q}_N(n) = \frac{\sum_{i=1}^{n-1} \mathbf{1}\{X_i = 0, X_{i+1} = 0\}}{(n-1)\,(1-\hat{P}_L(n-1))}.$$

Clearly, $\hat{P}_L(n)$, $\hat{U}(n)$ and $\hat{R}(n)$ are unbiased estimators, whereas $\hat{q}_L(n)$ and $\hat{q}_N(n)$ are biased, but the bias depends on the size of the samples. Moreover, if $\hat{P}_L(n)$ is consistent then the bias approaches 0 as $n \to \infty$ for both estimators.

1.6.4.2 Distribution of $\hat{P}_L(n)$

In this section, we want to express the distribution of $\hat{P}_L(n)$, or in other words, $P(\hat{P}_L(n) = i/n)$. This allows the computation of the variance of $\hat{P}_L(n)$. We have seen that this estimator is unbiased. If its variance approaches zero as the number of probes goes to infinity, then $\hat{P}_L(n)$ is consistent, or equivalently, $\hat{P}_L(n) \to P_L$ for $n \to \infty$.

The estimation of P_L at the nth probe sample is simply the ratio of the number of lost probes, i, over the total number of probes, n. For n samples, one may construct the

indefinitely. In the limiting case, as the sample size becomes infinite, a consistent estimator will provide a perfect point estimate of the target. In other words, an estimator is said to be consistent if and only if its bias and variance *both* approach zero, as $n \to \infty$.

vector $(X_1, \ldots, X_n)$ where $X_i = \mathbf{1}\{Q_i = K\}$. This vector takes on values from the set space $\{0,1\}^n$. For i lost packets, there are $C_n^i := C(n,i)$ possible values for $(X_1, \ldots, X_n)$, denote by $\mathcal{A}_i$ the set of these values. We can now write

$$\begin{aligned}
P\Big(\hat{P}_L(n) = i/n\Big) &= \sum_{(x_1,\ldots,x_n)\in\mathcal{A}_i} P\Big((X_1,\ldots,X_n) = (x_1,\ldots,x_n)\Big) \\
&= \sum_{(x_1,\ldots,x_n)\in\mathcal{A}_i} P(X_1 = x_1, \ldots, X_n = x_n) \\
&= \sum_{(x_1,\ldots,x_n)\in\mathcal{A}_i} P(X_n = x_n | X_1 = x_1, \ldots, X_{n-1} = x_{n-1}) \\
&\qquad \times P(X_{n-1} = x_{n-1} | X_1 = x_1, \ldots, X_{n-2} = x_{n-2}) \\
&\qquad \times \ldots \times P(X_2 = x_2 | X_1 = x_1) \times P(X_1 = x_1) \\
&= \sum_{(x_1,\ldots,x_n)\in\mathcal{A}_i} P(X_n = x_n | X_{n-1} = x_{n-1}) \times P(X_{n-1} = x_{n-1} | X_{n-2} = x_{n-2}) \\
&\qquad \times \ldots \times P(X_2 = x_2 | X_1 = x_1) \times P(X_1 = x_1) \qquad (1.86)
\end{aligned}$$

where exactly i variables x_j are equal to 1 and the remaining $n-i$ variables are equal to 0. To derive the last equality, we have used the memoriless property of the Markovian process $\{Q_n\}_n$. In order to simplify (1.86), introduce the following:

$a :=$ number of occurrences of two consecutive lost packets
$\quad =$ number of occurrences of the sequence '11' in $(x_1, \ldots, x_n)$
$b :=$ number of occurrences of two consecutive successful packets
$\quad =$ number of occurrences of the sequence '00' in $(x_1, \ldots, x_n)$
$c :=$ number of occurrences of a lost packet followed by a successful packet
$\quad =$ number of occurrences of the sequence '10' in $(x_1, \ldots, x_n)$
$d :=$ number of occurrences of a successful packet followed by a lost packet
$\quad =$ number of occurrences of the sequence '01' in $(x_1, \ldots, x_n)$

and

$$P_0 = \begin{cases} P_L, & \text{if } x_1 = 1, \\ 1 - P_L, & \text{if } x_1 = 0. \end{cases}$$

Obviously, the parameters a, b, c and d satisfy:

$$\begin{cases} a + b + c + d + 1 = n, \\ a + d + \mathbf{1}\{P_0 = P_L\} = i, \\ c = d, & \text{if } x_1 = x_n, \\ c = d + \mathbf{1}\{x_1 = 1, x_n = 0\} - \mathbf{1}\{x_1 = 0, x_n = 1\}, & \text{if } x_1 \neq x_n. \end{cases}$$

Notice that

$$\begin{aligned}
P(Q_k \neq K | Q_{k-1} = K) &= 1 - P(Q_k = K | Q_{k-1} = K) = 1 - q_L, \\
P(Q_k = K | Q_{k-1} \neq K) &= 1 - P(Q_k \neq K | Q_{k-1} \neq K) = 1 - q_N.
\end{aligned}$$

Equation (1.86) can now be rewritten as follows

$$P\Big(\hat{P}_L(n) = i/n\Big) = \sum_{(x_1,\ldots,x_n)\in\mathcal{A}_i} P_0(q_L)^a (q_N)^b (1-q_L)^c (1-q_N)^d. \tag{1.87}$$

At this point, we must distinguish between four different cases, according to whether the first packet and/or the last packet are lost or not.

- $x_1 = 0$ and $x_n = 0$. We have $P_0 = 1 - P_L$

$$i = 0 \Rightarrow \begin{cases} a = c = d = 0, \\ b = n-1. \end{cases}$$

$$1 \le i \le n-2 \Rightarrow \begin{cases} a = i - d, \\ b = n - i - d - 1, \\ c = d, \\ \text{with } d = 1, \ldots, \min(i, n-i-1). \end{cases}$$

  For each value of d, there are $C^d_{n-i-1} C^{d-1}_{i-1}$ different possible values for $(x_2, \ldots, x_{n-1})$ (Note: there are C^d_{n-i-1} ways of putting the d '0' of the sequence '01' in $n-i-1$ positions, and there are C^{d-1}_{i-1} possibilities for choosing $d-1$ cuts among all $i-1$ possible cuts in order to separate all the i 1's into d groups '01...1').

- $x_1 = 0$ and $x_n = 1$. We have $P_0 = 1 - P_L$

$$1 \le i \le n-1 \Rightarrow \begin{cases} a = i - d, \\ b = n - i - d, \\ c = d - 1, \\ \text{with } d = 1, \ldots, \min(i, n-i), \\ \text{or } c = 0, \ldots, \min(i-1, n-i-1). \end{cases}$$

  For each value of c, there are $C^c_{n-i-1} C^c_{i-1}$ different possible values for $(x_2, \ldots, x_{n-1})$ (Note: there are C^c_{n-i-1} ways of putting the c '0' of the sequence '10' in $n-2-(i-1)$ positions, and there are C^c_{i-1} possibilities for choosing c cuts among all $i-1$ possible cuts in order to separate all the i 1's into c groups '1...10' and the right-most group '1...1').

- $x_1 = 1$ and $x_n = 0$. We have $P_0 = P_L$

$$1 \le i \le n-1 \Rightarrow \begin{cases} a = i - d - 1, \\ b = n - i - d - 1, \\ c = d + 1, \\ \text{with } d = 0, \ldots, \min(i-1, n-i-1). \end{cases}$$

For each value of d, there are $C_{n-i-1}^{d} C_{i-1}^{d}$ different possible values for $(x_2, \ldots, x_{n-1})$ (Note: there are C_{n-i-1}^{d} ways of putting the d '0' of the sequence '01' in $n-2-(i-1)$ positions, and there are C_{i-1}^{d} possibilities for choosing d cuts among all $i-1$ possible cuts in order to separate all the i 1's into d groups '01...1' and the left-most group '1...1').

- $x_1 = 1$ and $x_n = 1$. We have $P_0 = P_L$

$$2 \leq i \leq n-1 \Rightarrow \left\{ \begin{array}{l} a = i-d-1, \\ b = n-i-d, \\ c = d, \\ \text{with } d = 1, \ldots, \min(i-1, n-i). \end{array} \right.$$

$$i = n \Rightarrow \left\{ \begin{array}{l} a = n-1, \\ b = c = d = 0. \end{array} \right.$$

For each value of c $(= d)$, there are $C_{n-i-1}^{d-1} C_{i-1}^{d}$ different possible values for $(x_2, \ldots, x_{n-1})$ (Note: there are C_{i-1}^{c} ways of putting the c '1' of the sequence '10' in $n-1-(n-i)$ positions, and there are C_{n-i-1}^{c-1} possibilities for choosing $c-1$ cuts among all $n-i-1$ possible cuts in order to separate all the $n-i$ 0's into c groups '10...0').

Finally, and after a factorization of the cases $x_1 \neq x_n$, (1.87) becomes

$$\begin{aligned} P\Big(\hat{P}_L(n) = i/n\Big) \;=\; & \mathbf{1}\{i=0\}(1-P_L)(q_N)^{n-1} + \mathbf{1}\{i=n\}P_L(q_L)^{n-1} \\ & + \mathbf{1}\{1 \leq i \leq n-2\} \sum_{d=1}^{\min(i,n-i-1)} C_{n-i-1}^{d} C_{i-1}^{d-1} (1-P_L)(q_L)^{i-d}(q_N)^{n-i-d-1}(1-q_L)^{d}(1-q_N)^{d} \\ & + \mathbf{1}\{1 \leq i \leq n-1\} 2P_L(1-q_L) \\ & \qquad \times \sum_{d=0}^{\min(i-1,n-i-1)} C_{n-i-1}^{d} C_{i-1}^{d} (q_L)^{i-d-1}(q_N)^{n-i-d-1}(1-q_L)^{d}(1-q_N)^{d} \\ & + \mathbf{1}\{2 \leq i \leq n-1\} \sum_{d=1}^{\min(i-1,n-i)} C_{n-i-1}^{d-1} C_{i-1}^{d} P_L(q_L)^{i-d-1}(q_N)^{n-i-d}(1-q_L)^{d}(1-q_N)^{d}. \end{aligned}$$

The variance of the estimator $\hat{P}_L(n)$ is simply

$$\mathrm{Var}\left[\hat{P}_L(n)\right] = \mathbf{E}\left[\left(\hat{P}_L(n)\right)^2\right] - \mathbf{E}\left[\hat{P}_L(n)\right]^2 = \sum_{i=0}^{n} (i/n)^2 \, P\left(\hat{P}_L(n) = i/n\right) - (P_L)^2.$$

It is quite hard to formally compute $\lim_{n\to\infty} \mathrm{Var}[\hat{P}_L(n)]$. Thus, we will rely on simulated results to compute the empirical variance of $\hat{P}_L(n)$ and further know whether or not this estimator is consistent. This is addressed in the next section.

1.6.4.3 Overall performance of the estimators

The overall performance of the estimators is presented in Table 1.3. In order to have a fair comparison between the estimators, we report their performance in $M+M/M/1/K$ simulations only. In these simulations, all the assumptions considered in Section 1.4.1 are satisfied. The performance of the estimators is thus affected by the speed of convergence solely.

Table 1.3: Overall performance of the estimators for 50000 probes and $M+M/M/1/K$ simulations: sample mean and percentiles of the relative error (expressed in percentage) and the empirical variance

	Relative error (%)					
Metric	Mean	25	50	75	90	95
P_L	5.07	0.52	2.86	6.46	11.9	21.9
U	0.17	0.002	0.09	0.27	0.51	0.68
R	0.46	0.03	0.07	0.59	1.43	2.43
q_L	10.7	0.55	5.76	11.4	18.8	57.8
q_N	0.20	0.01	0.11	0.24	0.60	0.90
	Empirical variance					
Metric	Mean	25	50	75	90	95
P_L	0.20	0.01	0.09	0.23	0.59	0.88
U	0.04	$9\,10^{-4}$	0.02	0.07	0.09	0.16
R	1.39	$3\,10^{-6}$	$2\,10^{-5}$	10^{-4}	0.004	13.1
q_L	19.6	0.13	1.06	15.2	91.1	115
q_N	0.35	0.003	0.05	0.30	1.37	2.25

For each experiment (20 different $M+M/M/1/K$ experiments have been conducted; see details in Section 1.7), we have computed the relative error (expressed in percentage) between each estimator in (1.81)–(1.85) and its corresponding theoretical value, as well as the variance of the estimato. This computation has been performed after the generation of 50000 probes. For a given estimator, we therefore have a collection of 20 values for the relative error as well as 20 values for the variance of the estimator.

Rows 3–7 in Table 1.3 report the mean and the percentiles of the relative error (expressed in percentage) using the collection of 20 values computed from the simulations, and rows 10–14 in the same table report the mean and the percentiles of the empirical variance of the estimators.

Estimator $\hat{q}_L$ is the least efficient estimator[5] since it has the largest empirical variance (see row 13 in Table 1.3). In other words, the estimator $\hat{q}_L$ is not good because it exhibits high variance. The distribution of $\hat{q}_L$ is not concentrated and the estimates of $\hat{q}_L$ vary too

[5]An estimator is said to be more efficient if it has a smaller variance. The distribution of an efficient estimator is highly concentrated.

much over time. We expect all schemes using $\hat{q}_L$ to perform badly. The rest of the estimators is more or less efficient, their distribution being highly concentrated. For $\hat{P}_L$, $\hat{U}$ and $\hat{R}$, we already now that they are unbiased (see Section 1.6.4.1), hence their distributions are said to be on target.

Looking now at rows 3–7 in Table 1.3, we see that the relative error of estimators $\hat{U}$, $\hat{R}$ and $\hat{q}_N$ is low, unlike the relative errors of $\hat{P}_L$ and $\hat{q}_L$. Thus, we expect all schemes using $\hat{P}_L$ to perform worse than the schemes using $\hat{R}$ for instance. However, this might not be the case due to the unexpected effect of combining several "noisy" estimators within the same scheme.

Remark 1.6.1 *Estimators $\hat{P}_L$, $\hat{q}_L$ and $\hat{q}_N$ are all loss-related and based on single-sided measurements, as these estimators are "naturally" available at the destination. Estimator $\hat{R}$ is based on an end-to-end measurement, as well as $\hat{U}$. One might expect that schemes involving both kind of metrics will perform better than schemes involving single-sided or end-to-end metrics solely, regardless of the performance of the metrics at hand.*

1.7 Simulation results and analysis

1.7.1 Trace generation

The data sets $\{a_i\}_i$, $\{d_i\}_i$, $\{X_i\}_i$ and $\{Y_i\}_i$ were extracted from traces generated by simulation models in `ns-2`. In this section, we report simulations in which there is a single queue to better observe the behavior of both inference models under various background traffic patterns. Simulations with multiple links are reported later on in Section 1.7.5. Overall, 50 simulations have been performed in which several types of background traffic are considered:

(T1) A Poisson flow of packets with exponentially distributed packet size. The average packet size is 100 Bytes.

(T2) A superposition of 100 Poisson-like flows. The inter-arrivals within each flow is exponentially distributed. The packet length is constant for each flow and its value is taken from an exponential distribution with average 100 Bytes. Therefore, different flows have different packet lengths.

(T3) An aggregation of 100 On/Off flows, where the On and Off times were taken from a Pareto distribution with shape 1.5. The packet length is constant for each flow and its value is taken from an exponential distribution with average 100 Bytes.

(T4) An aggregation of 250 On/Off flows, where the On and Off times were taken from a Pareto distribution with shape 1.5. The packet length is constant for each flow and its value is taken from an exponential distribution with average 100 Bytes.

(T5) An aggregation of 250 long-lived FTP over TCP flows.

(T6) An aggregation of 1000 long-lived FTP over TCP flows.

In all experiments foreground packets arrive according to a Poisson process and have exponentially distributed packet sizes (average = 100 Bytes) except in the case when the background traffic is of type (T2); in the latter case, the foreground source is also of type (T2).

It is important to specify, for each type of simulations, which assumptions are satisfied and which ones are violated.

- The set of simulations where the cross traffic is of type (T1) corresponds to the $M+M/M/1/K$ queue model. The interest of such simulations is to identify which scheme among schemes **I-X** converges faster.

- When both foreground and background traffic are of type (T2), the only assumption that is violated is the one concerning the service times. In these simulations, the service times are the same for each flow, but differ from flow to flow. There are a total of 101 different values coming all from an exponential distribution (the service time is proportional to the packet size). If the number of background flows is increased, the service time distribution will get closer to the exponential distribution. In this set of simulations, we are testing the robustness of both queue models against violation of the assumption on the service times.

- When the cross traffic is of type (T3) or (T4), the Poisson assumption for the background traffic is violated. The assumption on the distribution of the service times is also violated, but as the number of flows increases, the service time distribution will get closer to the exponential distribution (cf. previous item). However, when the number of flows grows to infinity, it is known that the aggregation of such On/Off flows will exhibit correlations across several time scales (see [116]). So, when the number of flows is increased, on one hand the assumption on the cross traffic will be *more* violated, and on the other hand the assumption on the service times will be *less* violated (case of the $M+M/M/1/K$ queue model). A comparison of the performance of the estimators when the background traffic is either (T3) or (T4) will help identify which assumption is more essential to the $M+M/M/1/K$ queue model.

- In the last set of assumptions (cross traffic of type (T5) or (T6)), the Poisson assumption for the background traffic is violated as well as the assumption of exponential service times. The FTP/TCP flows generate two kinds of packets: 512-Bytes data packets, and 40-Bytes acknowledgements. Thus, the service times of the background traffic take on two distinct values, whereas the service times of the foreground traffic are exponentially distributed. When the number of background flows is increased, the resulting distribution of the service times is expected to get farther from the exponential distribution. Going back to the background traffic assumption (which has

been made only for mathematical tractability), it is known from [95] that the arrivals within a single FTP flow are not Poisson. However, what we do not know is whether the distribution of the arrivals from an *aggregation* of several FTP flows approaches the exponential distribution or not. We can say that, *a priori*, the assumption on the background arrivals is violated, and we are tempted to add: as the number of exogenous flows increases, the distribution of the resulting inter-arrival process gets closer to the exponential distribution.

Let us now return to the description of the traces generated. The rate of the foreground traffic (the probes) was equal to 250 pkts/s in all experiments (except in case (T1) where values of 125, 250 and 500 pkts/s were retained). On the network side, the server rate was either equal to 1500 pkts/s or to 6500 pkts/s and the buffer size was either equal to 10, 30, 65, 100, 150 or to 1000 packets (recall that in `ns-2` the size of the buffer is defined in number of packets regardless of their size).

Below, we give the ranges of values obtained for the five metrics over all 50 experiments:

- P_L ranged from 1.7×10^{-4} to 0.637
- U ranged from 0.892 to 1
- R ranged from 0.0007 to 0.66 seconds
- q_L ranged from 0.105 to 0.64
- q_N ranged from 0.367 to 0.9998.

As for the rate of exogenous traffic intensity λ, measured as the number of background packets arriving to the bottleneck link over the run time, its value ranged from 1593.2 to 17437 packets per second, giving the range 0.965 – 2.758 for the traffic intensity ρ. Notice that in all the simulations, the single link was (highly) congested.

1.7.2 Estimating cross traffic rate, buffer size and (possibly) server capacity

Having at our disposal $\{a_i\}_i$, $\{d_i\}_i$, $\{X_i\}_i$ and $\{Y_i\}_i$ for the n first probing packets, the moment-based estimators are computed according to formulas (1.81), (1.82), (1.83), (1.84) and (1.85). At this point, $\hat{P}_L(n)$, $\hat{U}(n)$, $\hat{R}(n)$, $\hat{q}_L(n)$ and $\hat{q}_N(n)$ are substituted into (1.3), (1.5), (1.10), (1.18), (1.21), (1.37), (1.38) and (1.40). The ten triples of equations referred to as schemes *1* through *10* and the eleven pairs of equations referred to as schemes **I** through **XI** are then solved numerically using a C program including the NAG[6] C library [90, 91]. Results are reported in Tables 1.3–1.9 and Figures 1.11–1.15.

[6]NAG is a copyright of The Numerical Algorithms Group Ltd

1.7.3 Analysis of the results in case μ is known

In this section, we restrict ourselves to the estimation of parameters λ and K, thereby assuming that μ is known. We briefly discuss the results returned by schemes **I** through **XI** (each involving two QoS metrics) and then focus on the performance of the "best" scheme.

Our findings can be summarized as follows:

- Schemes **III**, **IV** and **X** give almost identical results. This is not surprising, though, since the three of them involve loss-related metrics which are related by (1.22) as seen in Section 1.4.6. We further observed that their solutions always under-estimate the correct values. We believe that this is due to a lack of information as these schemes count on loss-related measurements solely (variables $\{X_n\}_n$ introduced in Section 1.4.2).

- Schemes **I** $= P_L\_U$ and **VII** $= U\_q_N$ return similar results as do schemes **II** $= P_L\_R$ and **IX** $= R\_q_N$. Notice that both pairs of schemes have a common metric (U for the first pair and R for the second one) and the second metric is either P_L (schemes **I** and **II**) or q_N (schemes **VII** and **IX**). It appears that interchanging P_L and q_N has little impact on the performance of a scheme, even though the latter metric is much better estimated than the former one (cf. Section 1.6.4.3).

- Schemes **VI** and **VIII** performed poorly, either returning bad estimates $\hat{\lambda}$ and $\hat{K}$ or even not returning results at all. This is due to the fact that these schemes involve q_L, which was seen to be badly estimated (cf. Section 1.6.4.3).

- The solution returned by scheme **V** always over-estimates the true values. This scheme involve metrics U and R which can both be seen as end-to-end measurements. These metrics provide somehow redundant informations which can explain the bad performance of the scheme.

- All schemes including U saw their performance degrade as the network become more congested. When the single queue is congested, its buffer does not empty often. As a result the first estimates of U are $\hat{U} = 1$, which is not a valid value in either model. As soon as a probe packet finds an empty queue, the first *valid* estimate of U is computed, and it is then and only then that the schemes using U can return a solution. Since in our simulations we considered only congested cases, all schemes including U suffered from this discrepancy and their results were not the best ones.

- Scheme **XI** returns the same estimate $\hat{\lambda}$ as does scheme **I**. Both schemes involve metrics P_L and U, but the first one derive from the $M/D/1/K$ model whereas the second one come from the $M/M/1/K$ model. However, the formulas giving $\hat{\lambda}$ are identical (see Equations (1.50) and (1.79)). As for the buffer size K, it is much better estimated using scheme **I**. The cause behind the misestimation of K when using scheme **XI**

is the misestimation of U. Even though scheme **I** involves U as well, scheme **XI** is much more sensitive to the value of $\hat{U}$. Recall that K is estimated as the integer j for which $\alpha_j(\rho)$ is the closest to $(1-\hat{P}_L)/(1-\hat{U})$ (cf. Section 1.6.2.6). In congested cases, $\hat{U}$ is almost 1 and a small deviation from the true value leads to a large error in $(1-\hat{P}_L)/(1-\hat{U})$ (e.g. if $\hat{U} = 1-10^{-5}$ and $U = 1-10^{-4}$ then $\alpha_{\hat{K}}(\rho) = 10\alpha_K(\rho)$, resulting in $\hat{K} > K$).

Now that we have discussed the averall results for all eleven schemes, we will focus on the best scheme, scheme **II** $= P_L\_R$. We have mentioned before that schemes P_L_R and R_q_N gave similar results but that the former scheme performed slightly better. Notice that both schemes combine the use of a single-sided measurement (P_L or q_N) and an end-to-end measurement which is R. These schemes contain the least redundant information, (as opposed to scheme $P_L\_q_N$, for instance). From now on, only results pertaining to scheme P_L_R are presented.

Tables 1.4, 1.5, 1.6 and 1.8 report the relative error (expressed in percentage) between the estimate of parameter λ (resp. K), denoted as $\hat{\lambda}$ (resp. $\hat{K}$), returned by scheme P_L_R and the measured value λ (resp. the true value K), for various cross traffic patterns (Poisson traffic as defined in (T1) in Table 1.4, Poisson-like flows as defined in (T2) in Table 1.5), a superposition of On/Off sources with Pareto On and Off time distribution as defined in (T3)-(T4) in Table 1.6, a superposition of FTP/TCP flows as defined in (T5)-(T6) in Table 1.8.

Table 1.4: Relative error (expressed in percentage) of the estimates for 50000 probes returned by the scheme P_L_R, when the cross traffic is a single Poisson source

		Simulation parameters			
		$\lambda = 6600$	$\lambda = 6600$	$\lambda = 6600$	$\lambda = 17068$
		$\gamma = 124$	$\gamma = 248$	$\gamma = 496$	$\gamma = 125$
		$\mu = 6968$	$\mu = 6968$	$\mu = 6967$	$\mu = 6962$
Buffer size	Estimator	$\rho = 0.965$	$\rho = 0.983$	$\rho = 1.019$	$\rho = 2.470$
$K = 10$	$\hat{\lambda}$	0.6	0.004	0.1	0.1
	$\hat{K}$	0.7	0.9	1.4	0.4
$K = 30$	$\hat{\lambda}$	0.1	0.1	0.3	0.9
	$\hat{K}$	0.7	1.6	0.6	0.05
$K = 65$	$\hat{\lambda}$	0.04	0.2	0.7	1.0
	$\hat{K}$	1.1	1.0	0.3	0.1
$K = 100$	$\hat{\lambda}$	0.04	0.1	0.1	0.5
	$\hat{K}$	2.8	2.7	0.2	0.01
$K = 150$	$\hat{\lambda}$	0.1	0.1	0.02	0.2
	$\hat{K}$	8.3	4.1	0.4	0.03

Table 1.4 shows excellent results regarding the estimation of λ (obtained after 50000 probes). The relative error on $\hat{\lambda}_{50000}$, computed as $|\hat{\lambda}_{50000} - \lambda|/\lambda$, is always below 1.0% in all the simulations reported in Table 1.4 (see rows 6, 8, 10, 12 and 14). As for the estimation of K, the results are very good for moderate values of K: the relative error on $\hat{K}_{50000}$, computed as $|\hat{K}_{50000} - K|/K$, is always below 1.6% when $K \leq 65$ (see rows 7, 9 and 11 in Table 1.4). For larger values of K, the speed of convergence depends on the load ρ. As ρ increases from 0.965 (third column) to 2.470 (column 6), the relative error on K decreases for $K \geq 65$ (see rows 11, 13 and 15). Notice that in any case the estimates should converge to the true values as the number of probes increases since the experiments considered in Table 1.4 simulate at best the $M/M/1/K$ queue.

The speed of convergence of $\hat{\lambda}$ can be observed in Figure 1.11, where the evolution of the estimated cross traffic intensity is plotted against the number of probes for several values of the load ρ. For ρ around 1, the estimation converges after approximately 10000 probes (see Figures 1.11(a)-(c)) whereas 5000 probes are enough for $\rho = 2.470$ (see Figure 1.11(d)).

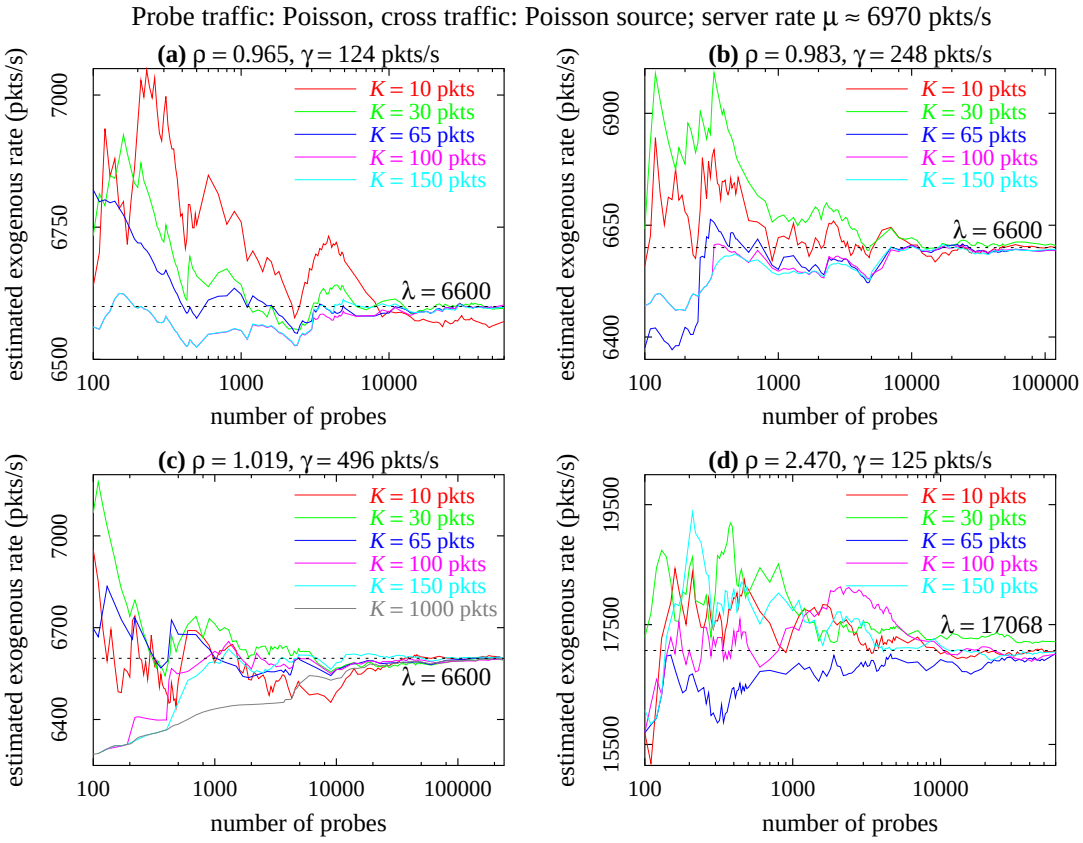

Figure 1.11: Evolution of the estimated cross traffic intensity vs. the number of probes

The slower convergence of $\hat{K}$ for smaller values of ρ can be observed in Figure 1.12

where the evolution of the estimated buffer size is plotted against the number of probes for several values of K. It is clearly visible in Figures 1.12(c)-(d) that $\hat{K}$ converges faster to K as ρ increases. Notice also the fast convergence of $\hat{K}$ to the true value for $\rho = 2.470$ in all four cases shown in Figure 1.12 ($K = 10, 30, 65, 100$).

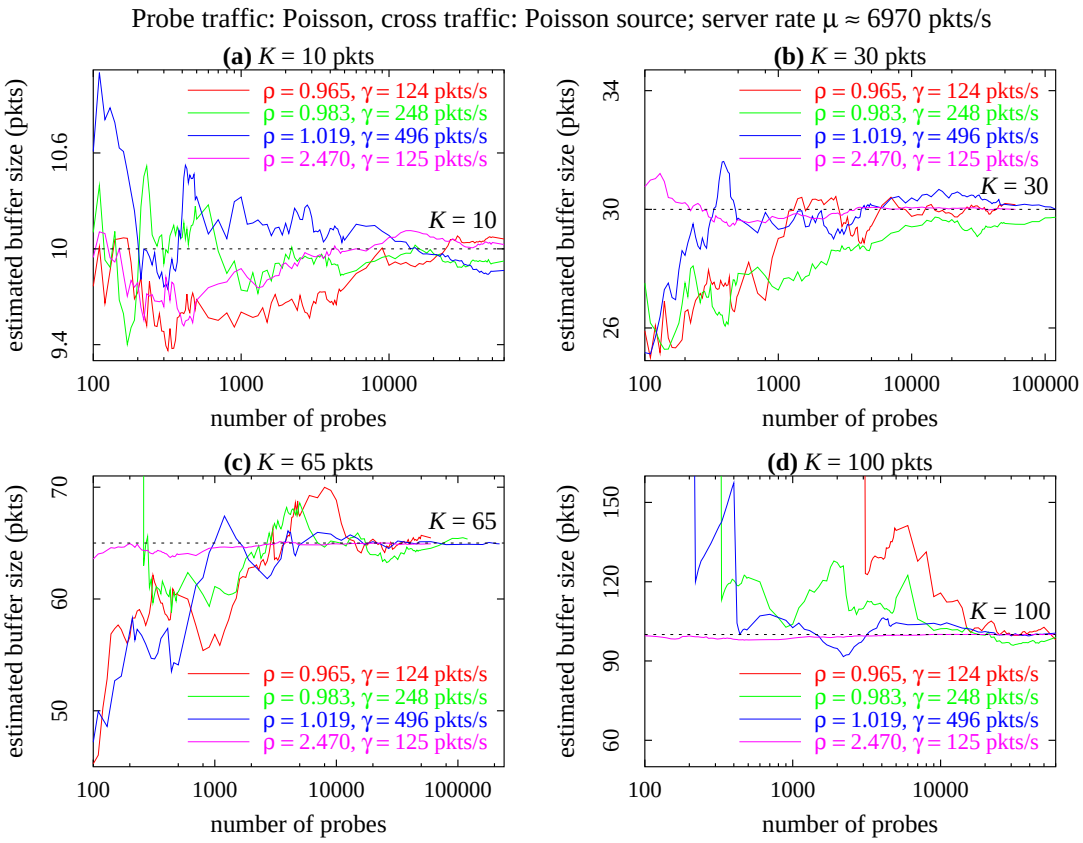

Figure 1.12: Evolution of the estimated buffer size vs. the number of probes

Consider now the set of simulations where all sources (i.e. foreground *and* background sources) are Poisson-like (type (T2)). We have seen before that this set of simulations undertakes the robustness of both models to violation of the assumption on the distribution of the service times. The relative error (expressed in percentage) is reported in Table 1.5. We observe that both λ and K are better estimated as K increases. In all cases, $\hat{\lambda}$ stays

Table 1.5: Relative error (expressed in percentage) of the estimates (scheme P_L_R) for 120000 probes: Poisson-like flows, $\lambda = 6677$, $\gamma = 250$, $\mu = 6374$ and $\rho = 1.087$

Estimator	$K = 10$	$K = 30$	$K = 65$	$K = 100$	$K = 150$
$\hat{\lambda}$	3.1	1.1	0.04	0.1	0.1
$\hat{K}$	9.2	8.5	6.9	5.4	4.0

within 3.1% of the true value (cf. row 2 in Table 1.5) such as λ is overestimated, whereas $\hat{K}$ stays within 9.2% of the true value (cf. row 3 in Table 1.5) such as K is underestimated.

The estimation of K is not as satisfactory as the estimation of λ. It is clear that the quality of $\hat{\lambda}$ and $\hat{K}$ is influenced by the quality of estimators $\hat{P}_L$ and $\hat{R}$. Our next step is to look at the performance of these estimators. We will compute the loss probability P_L and the expected response time R as expected by the $M{+}M/M/1/K$ model using the true values of λ and K. The resulting values of P_L and R are then compared to the estimated values. A small error between both pairs of values implies a small error in $\hat{\lambda}$ and $\hat{K}$ as predicted by scheme P_L_R. Our findings can be summarized as follows.

- The loss probability predicted by the model, P_L, is smaller than the estimated $\hat{P}_L$. The absolute deviation of the predicted P_L (defined as $|P_L - \hat{P}_L|$) decreases from 0.025 (16.3% of relative deviation[7]) for $K = 10$ down to 0.002 (2.8% of relative deviation) for $K = 150$.
- The expected response time predicted by the model, R, is slightly larger than the estimate $\hat{R}$. The deviation of the predicted R increases from $57\mu s$ (6.3% of mismatch) for $K = 10$ up to $871\mu s$ (4.2% of mismatch) for $K = 150$.
- The $M{+}M/M/1/K$ model predicts much better the response time R than the loss probability P_L.

It seems that the error in estimating K is due to the error between P_L and $\hat{P}_L$, and that both the error on K and the (small) one on λ vary as does the error on $\hat{P}_L$. It is also possible that the errors at hand are also affected by the error on $\hat{R}$, but this impact (if it exists) is negligible both because of the small error on $\hat{R}$ and because of the large relative error on $\hat{P}_L$.

Remark 1.7.1 *The preceding observations describe the sensitivity of $\hat{\lambda}$ and $\hat{K}$ to variations in $\hat{P}_L$ and $\hat{R}$.*

The values that are given in Table 1.5 were computed for 120000 probes. The evolution of the estimates over the number of probes is plotted in Figure 1.13. Observe in Figure 1.13(a) how the estimate $\hat{\lambda}$ for $K = 10$ converges above the dashed line which represents the true value to be estimated. The same is true for $K = 30$. For $K = 65, 100, 150$, the estimate $\hat{\lambda}$ converges to the correct value. The reason why, for small K, $\hat{\lambda}$ overestimates λ, is that $\hat{P}_L$ is larger than the P_L predicted by the model ($\hat{R}$ being close to R for small

[7]The relative deviation between two values X and $\hat{X}$ is defined as $|X - \hat{X}|/\hat{X}$ and is sometimes called *mismatch*.

K). Recall that in the $M/M/1/K$ queue, when the load increases/decreases, both the loss probability and the response time increase/decrease. For large values of K, we have seen that $\hat{P}_L$ is slightly larger than P_L (2.8% of mismatch) and that $\hat{R}$ is slightly smaller than R (4.2% of mismatch). Each mismatch induces an error on $\hat{\lambda}$, but since the induced errors are in opposite directions, the final result is that $\hat{\lambda}$ is on target (cf. plots for $K = 65, 100, 150$ in Figure 1.13(a)).

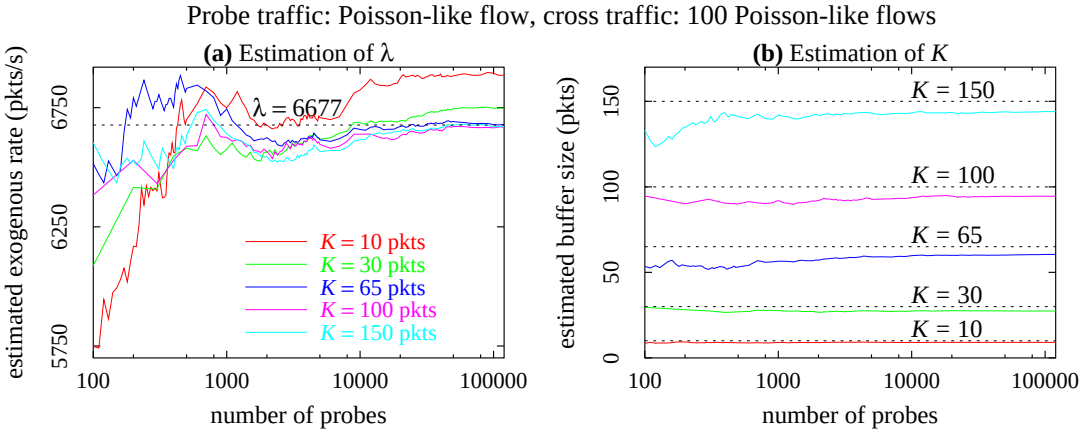

Figure 1.13: Evolution of the estimates vs. the number of probes

Figure 1.13(b) depicts the variations of the estimates for K as a function of the number of probes. Even though the absolute error ($|\hat{K}-K|$) between each plot and its corresponding dashed line increases as K increases, the relative error ($|\hat{K}-K|/K$) *decreases*. Observe that K is always underestimated, which is expected since $\hat{P}_L > P_L$ and $\hat{R} < R$. If the size of the buffer in the $M/M/1/K$ queue decreases, the loss probability P_L increases whereas the response time decreases. The mismatch of both metrics induces a larger error on K than the one induced on λ, as both mismatches result in underestimating K. Notice how "flat" are the plots in Figure 1.13(b), especially when compared to the bursty plots in Figure 1.12. Finally, convergence takes place with approximately 10000 probes when estimating λ, and even fewer when estimating K.

Of more interest are the results in Tables 1.6 and 1.8, since they have been obtained when the assumption that the cross traffic is Poisson is violated. We see that the quality of the estimates increases as the number of sources increases, or equivalently, when the load ρ increases (results obtained after 120000 probes). We will discuss first the results obtained when the cross traffic is the aggregation of On/Off flows (cf. Table 1.6) and come back later on to the case where the cross traffic is the aggregation of TCP flows (cf. Table 1.8).

For 100 On/Off sources (see rows 3–4 in Table 1.6), all estimates for λ are within 6% of the correct value, which is a satisfactory result. The relative error on $\hat{\lambda}$ seems to increase for $K \leq 65$ and decrease for $K > 65$ whereas the relative error on $\hat{K}$ definitely increases as

Table 1.6: Relative error (expressed in percentage) of the estimates (scheme P_L_R) for 120000 probes: cross traffic is of type (T3) and (T4) (On/Off flows)

	100 sources: $\lambda = 6812$, $\gamma = 247$, $\mu = 6663$ and $\rho = 1.059$				
Estimator	$K = 10$	$K = 30$	$K = 65$	$K = 100$	$K = 150$
$\hat{\lambda}$	3.8	5.2	6.0	5.4	4.7
$\hat{K}$	7.5	17.7	29.5	31.4	33.2
	250 sources: $\lambda = 17437$, $\gamma = 246$, $\mu = 6532$ and $\rho = 2.707$				
Estimator	$K = 10$	$K = 30$	$K = 65$	$K = 100$	$K = 150$
$\hat{\lambda}$	1.0	0.6	0.6	0.4	0.05
$\hat{K}$	1.1	0.5	0.4	0.4	0.1

the buffer size increases. For 250 On/Off sources (see rows 7–8 in Table 1.6), the results are much more satisfactory with all estimates for λ (resp. K) lying within 1% (resp. 1.1%) of the correct value. Notice that the relative error on both $\hat{\lambda}$ and $\hat{K}$ decreases as K increases. Searching for an explanation on these observations, we investigated on the performance of $\hat{P}_L$ and $\hat{R}$ in these particular simulations, and observed the following.

- For 100 On/Off sources ($\rho = 1.059$), the measured loss probability decreases from 0.16 for $K = 10$ down to 0.09 for $K = 150$, whereas the loss probability predicted by the model decreases from 0.13 to 0.05 as K increases and is smaller than the measured $\hat{P}_L$. The absolute deviation on P_L increases from 0.03 up to 0.05 for $10 \leq K \leq 65$ and decreases from 0.05 to 0.02 for $65 \leq K \leq 150$. The mismatch between the two values is not negligible (between 16.7% and 47.6%). As K increases, the response time predicted by the model increases from $0.94ms$ to $19.7ms$; $\hat{R}$ is smaller than the predicted R, increasing from $0.91ms$ to $13.5ms$. The deviation between the two values grows from $34\mu s$ (3.8% of mismatch) up to $6.2ms$ (45.9% of mismatch).

- For 250 On/Off sources ($\rho = 2.707$), both the predicted loss probability and the measured one are approximately constant and equal to 0.63, having the former being slightly larger than the latter (0.56% of maximum mismatch). The negligible deviation on P_L is always decreasing as K increases. As for the response time, the prediction returned by the $M{+}M/M/1/K$ model increases from $1.45ms$ to $22.90ms$ as K increases. As for the measured $\hat{R}$, it increases from $1.43ms$ to $22.87ms$ as K increases. The deviation between the two values is really negligible, of the order of tens of microseconds.

We can deduce from the above observations that for 100 On/Off sources ($\mu = 6663$), the error on $\hat{\lambda}$ varies as does the deviation between $\hat{P}_L$ and P_L; and that the error on $\hat{K}$ varies as does the deviation between $\hat{R}$ and R. For 250 On/Off sources ($\mu = 6532$), the errors on $\hat{\lambda}$ and $\hat{K}$ follow mainly the variations of the deviation between $\hat{P}_L$ and P_L.

Figure 1.14 depicts the evolution of the estimates as a function of the number of probes. Looking at Figure 1.14(a) (resp. Figure 1.14(b)), it appears that, for all K's, the estimator $\hat{\lambda}$ converges after 1000 probes (resp. 3000 probes) when the number of background flows is 100 (resp. 250). We observe in Figure 1.14(a) that the estimates deviate from the true value as K goes from 10 to 65, and get closer to $\lambda = 6812$ as K goes from 65 to 1000. The estimates for K are quite bursty (see Figures 1.14(c)-(f)). The estimates corresponding to 250 sources stay close to the true values (dashed line in each graph), while the ones corresponding to 100 sources considerably underestimate the true values as K increases. The causes of such underestimation (31.4% of error for $K = 100$) are twofold: first, $\hat{R} < R$, and second, $\hat{P}_L > P_L$. Recall that in a $M/M/1/K$ queue, decreasing the buffer size increases the loss probability and decreases the response time, which explains why such deviations in the values of P_L and R lead to an underestimation of K.

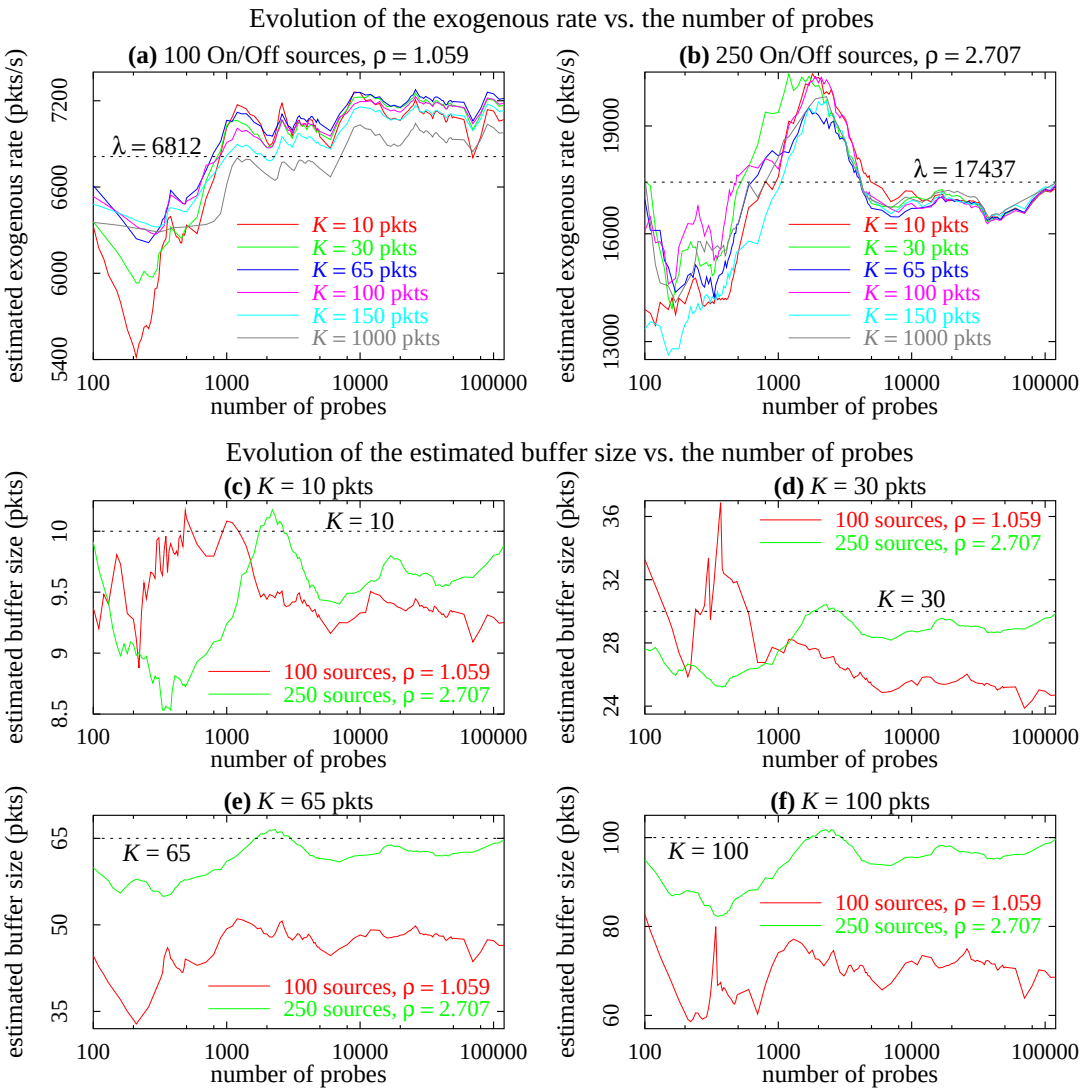

Figure 1.14: Probe traffic: Poisson, cross traffic: On/Off flows, Pareto On/Off times

To complete the discussion of the set of simulations where the cross traffic is of type (T3) or (T4), we will try to explain why scheme P_L_R behaves much better when there are 250 background sources rather than just 100 sources (for large K, the difference in performance between both cases is even more important). For each type of cross traffic, we have computed the Hurst parameter as well as the autocorrelation for both the interarrival sequence of the cross traffic and the service times sequence[8]. We have also tested the exponential distribution hypothesis of both sequences, using the goodness of fit test[9] [120]. Table 1.7 summarizes our findings. We have seen that the mismatch between the measured metrics and the predictions returned by the model drastically decreases when the number of background sources grows from 100 to 250 (see rows 12–13 in Table 1.7). We have not found any important difference in the characteristics of the cross traffic interarrivals sequence nor in the service times sequence when the number of sources increases (see rows 4–6, 8–10 in Table 1.7), which is not the case of the load (see second row in Table 1.7). We believe that the large value of ρ is behind the good performance of scheme P_L_R when there are 250 background sources. When the load is large, the queue does not empty often leading to a high number of lost packets and to a response time which is approximately the same

Table 1.7: Summary

Criterion	100 On/Off sources	250 On/Off sources
Rate	1.059	2.707
Cross traffic interarrivals sequence		
Distribution	slightly closer to an exponential when 250 sources	
Autocorrelation	slightly less autocorrelation when 250 sources	
Hurst parameter	0.805849	0.811553
Service times sequence		
Distribution	slightly closer to an exponential when 250 sources	
Autocorrelation	less autocorrelation when 250 sources	
Hurst parameter	0.837137	0.831835
Mismatch (in %) at 120000 packets	min, avg, max	min, avg, max
between P_L and $\hat{P}_L$	16.7, 37.1, 47.6	0.04, 0.26, 0.6
between R and $\hat{R}$	3.8, 28.4, 45.9	0.07, 0.45, 1.3

[8] In [35], the author provides practical instructions on how to compute the autocorrelation and the Hurst parameter using C programs, which are available at [34]

[9] For a descriptive derivation of the test, the N observed values of a sequence are ordered from smallest to largest. Denote as $x_{(i)}$ the observed value coming in the ith position. If the data really do come from an exponential distribution with parameter r, then we would expect the points $(1-\exp(-rx_{(i)}), i/(N+1))$ to be close to the diagonal line $y = x$; conversely, strong deviation from this line is evidence that the distribution did not produce the data.

for all packets. We believe that, in this case, the measured values of the metrics are close to the actual values (which are close to those predicted by the model, even though some assumptions are violated), which is not the case for 100 sources.

We will now analyze the results of the set of simulations in which the cross traffic is of type (T5) and (T6) (FTP over TCP flows). The relative error of the estimates are reported in Table 1.8. For 250 FTP/TCP flows, we observe the same thing as for 100 On/Off sources: the relative error on $\hat{\lambda}$ increases for $K \leq 65$ and decreases for $K > 65$, but here, the relative error on $\hat{K}$ is *decreasing* as the buffer size increases (refer to rows 4–5 in Table 1.8). However, in the case where there are 1000 FTP/TCP flows (see rows 9–10 in Table 1.8), both estimators present a relatively constant error. Furthermore, all estimates for λ (resp. K) are within 3.2% (resp. 0.6%) of the correct values, which is a good result.

Remark 1.7.2 *One characteristic of the set of simulations where the cross traffic is of type (T5) or (T6) is that the cross traffic intensity λ depends on the buffer size K. This is due to the fact that TCP is a closed-loop protocol. The cross traffic intensity is reported in rows 3 and 8 in Table 1.8.*

Table 1.8: Relative error (expressed in percentage) of the estimates (scheme P_L_R) for 120000 probes: cross traffic is of type (T5) and (T6) (FTP/TCP flows)

	250 sources: $\gamma = 248$, $\mu = 1502$ and $\rho = 1.258$				
	$K = 10$	$K = 30$	$K = 65$	$K = 100$	$K = 150$
Estimator	$\lambda = 1655$	$\lambda = 1661$	$\lambda = 1656$	$\lambda = 1642$	$\lambda = 1593$
$\hat{\lambda}$	7.0	7.6	8.3	7.6	6.7
$\hat{K}$	5.9	2.2	1.0	1.4	1.3
	1000 sources: $\gamma = 248$, $\mu = 1491$ and $\rho = 1.421$				
	$K = 10$	$K = 30$	$K = 65$	$K = 100$	$K = 150$
Estimator	$\lambda = 1883$	$\lambda = 1881$	$\lambda = 1882$	$\lambda = 1881$	$\lambda = 1820$
$\hat{\lambda}$	2.8	3.2	3.0	3.2	3.0
$\hat{K}$	0.5	0.04	0.4	0.6	0.6

We will try as before to identify what lies behind these observations. We looked at the performance of $\hat{P}_L$ and $\hat{R}$ in all the simulations in which the cross traffic is the aggregation of FTP over TCP flows, and found that:

- For 250 FTP/TCP sources, the absolute deviation between the measured $\hat{P}_L$ and the predicted P_L increases for $K \leq 65$ and decreases for $K \geq 65$, staying in the range 0.041 – 0.054 (mismatch in the range 15.3% – 20.2%), such that $\hat{P}_L > P_L$. The response time predicted by the model is quite close to the measured $\hat{R}$, the absolute deviation is in the range $0.11ms$ – $0.59ms$ and the mismatch is in the range 0.47% – 2.3%.

- For 1000 FTP/TCP sources, both metrics have a relatively stable mismatch, the one on P_L (resp. on R) being around 5.96% (resp. 0.57%). As before, $\hat{P}_L > P_L$.

In this set of simulations, it appears that the error on $\hat{\lambda}$ varies as does the error on $\hat{P}_L$; and that the error on $\hat{K}$ varies as does the error on $\hat{R}$. When the mismatch of $\hat{P}_L$ (resp. of $\hat{R}$) does not vary much for different values of K (given the same number of probes), the estimates of λ (resp. of K) will be approximately constant.

To observe the speed of convergence of the estimates, the reader is invited to look at Figure 1.15. In Figures 1.15(a)-(b), the evolution of the estimates of λ is plotted against the number of probes. Surprisingly enough, the estimates converge rather quickly. The convergence occurs around 2000 probes for all values of K and for both types of cross traffic ((T5) and (T6)), it is even faster than in the case of Poisson background traffic (see Figure

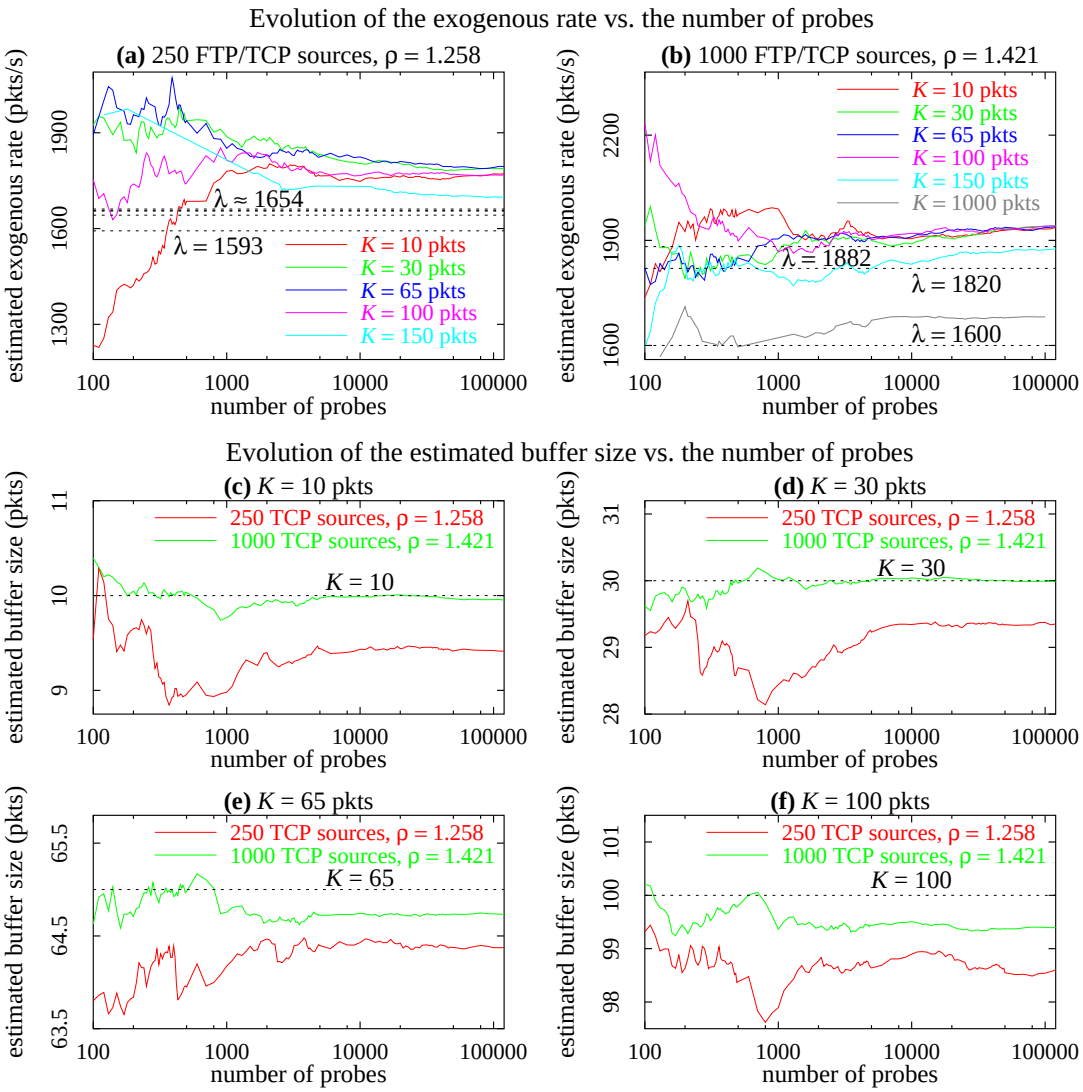

Figure 1.15: Probe traffic: Poisson, cross traffic: FTP/TCP sources

1.11). We observe the same speed of convergence of the estimates for K (between 2000 and 5000 probes, see 1.15(c)-(f)). We can also observe how the estimates are right on target when there are 1000 TCP flows. In the case where there are 250 TCP flows, $\hat{K}$ slightly underestimates K. The reason is that $\hat{P}_L > P_L$. Another effect of such mismatch is the overestimation of λ as observed in Figures 1.15(a)-(b).

As in the previous set of simulations, the predicted P_L returned by the model approaches the measured $\hat{P}_L$ when the load increases, resulting in a better performance for scheme PL_R.

Finally, we report the performance of scheme P_L_R over all 50 simulations (each simulation lasts exactly 500 seconds). Figure 1.16 displays the complementary cumulative distribution function (CCDF) of the relative error returned by estimates $\hat{\lambda}$ and $\hat{K}$. We observe that estimate $\hat{\lambda}$ returns more accurate results compared to $\hat{K}$, as the tail of the CCDF of the error on K is longer than the tail on the CCDF of the error on λ.

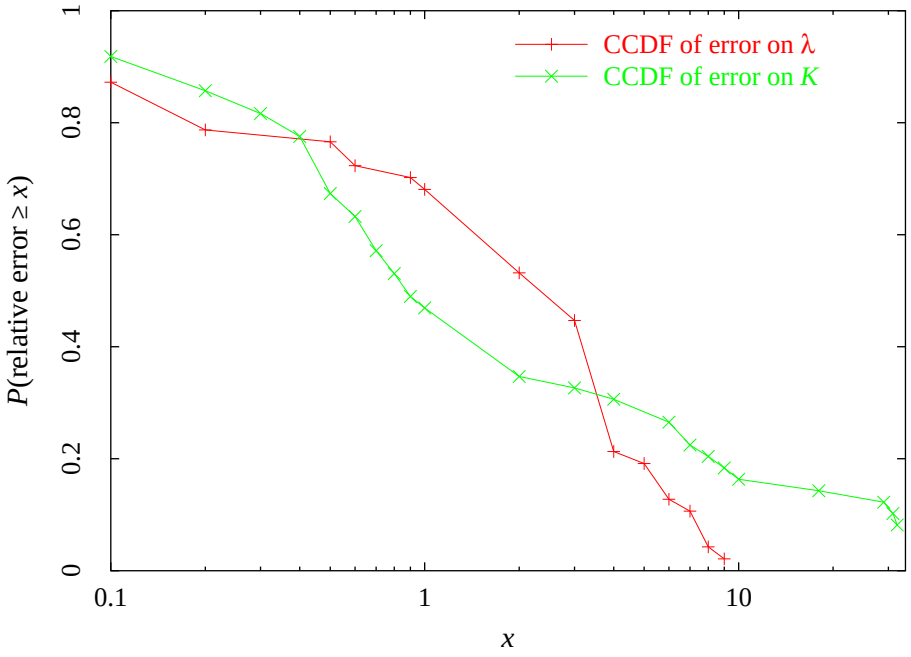

Figure 1.16: The complementary cumulative distribution function of the relative error returned by estimates $\hat{\lambda}$ and $\hat{K}$

In Table 1.9 we classify the results according to some specific performance criterion. For instance, we see from this table that the estimate for λ (resp. K) is within 9% of the exact value in 98% (resp. 84%) of the experiments. Only for large values of K ($K \geq 1000$) the scheme works poorly and may return no value for $\hat{K}$.

From this experimental study we conclude that the inference model $M+M/M/1/K$

Table 1.9: Percentage of hits for scheme P_L_R over the simulations

Criterion	Percentage of hits over the simulations
$\hat{\lambda}$, error within 1 %	52 %
$\hat{K}$, error within 1 %	40 %
$\hat{\lambda}$, error within 5 %	76 %
$\hat{K}$, error within 5 %	70 %
$\hat{\lambda}$, error within 9 %	98 %
$\hat{K}$, error within 9 %	84 %
bad estimation for λ	2 %
bad estimation for K	10 %
no estimation for K	6 %

returns reasonably good results even when the Poisson assumption on the background traffic and the assumption on the service times are violated. We have seen that, in general, the scheme P_L_R performs better under high load, returning good estimates for both λ and K.

1.7.4 Analysis of the results in case μ is unknown

We were not surprised to see that scheme *1* $= P_L\_U\_R$ was the "best" scheme in simultaneously estimating the cross traffic intensity λ, the server rate μ and the buffer size K. Even though this scheme was the "best", it returned results only in 31 simulations among all 50. Since this scheme uses an estimate of the utilization U, all simulations where the queue never emptied (there were 19 such simulations) did not lead to any valid estimate of U. (Recall that the value $U = 1$ is not valid in both models.) Table 1.10 lists the simulations in which the queue emptied at least once.

Table 1.10: The 31 simulations where $\hat{U} < 1$

Probe traffic		Cross traffic			
Type	Rate (pkts/s)	Type	Rate (pkts/s)	Buffer size K (pkts)	Simulations
(T1)	$\gamma = 124$	(T1)	$\lambda = 6600$	10, 30, 65, 100, 150	5
(T1)	$\gamma = 248$	(T1)	$\lambda = 6600$	10, 30, 65, 100, 150	5
(T1)	$\gamma = 496$	(T1)	$\lambda = 6600$	10, 30, 65, 100, 150, 1000	6
(T1)	$\gamma = 125$	(T1)	$\lambda = 17068$	10	1
(T2)	$\gamma = 250$	(T2)	$\lambda = 6677$	10, 30, 65, 100, 150	5
(T1)	$\gamma = 247$	(T3)	$\lambda = 6812$	10, 30, 65, 100, 150, 1000	6
(T1)	$\gamma = 246$	(T4)	$\lambda = 17437$	10	1
(T1)	$\gamma = 248$	(T5)	$\lambda = 1655$	10	1
(T1)	$\gamma = 248$	(T6)	$\lambda = 1883$	10	1

We will not discuss much the results returned by scheme $P_L\_U\_R$, as the latter does not perform especially well. The relative error (computed after 60000 probes) on λ (resp. on μ, on K) was below 4.98% (resp. below 4.72%, below 3.23%) in 17 simulations: the ones listed in rows 3–6 (except for $K = 1000$) and row 9 in Table 1.10. The relative error on each parameter is not negligible in the other 14 simulations (even after 120000 probes). The smallest error on λ (resp. on μ, on K) is 18.3% (resp. 18.4%, 22.1%), the average error on λ (resp. on μ, on K) is 75.0% (resp. 68.9%, 65.2%) and the largest error on λ (resp. on μ, on K) is 151.5% (resp. 126.4%, 102.9%)! In other words, the scheme behaves well almost only in $M+M/M/1/K$ simulations (rows 3–6 in Table 1.10). This statement is somehow biased since we have simulated congested cases solely ($\rho \in [0.965, 2.758]$). It is likely that for moderate values of ρ, the utilization will be better estimated, which will imply a better performance of scheme $P_L\_U\_R$.

1.7.5 Simulations with several links

We have seen that scheme P_L_R is the most promising one in estimating the cross traffic intensity λ and the buffer size K. Until now, we have tested this scheme on simulations in which there was only one single link. In this section, we briefly present the results returned by scheme P_L_R when applied on simulations with multiple links.

We have simulated six different scenarios all having the same network topology as illustrated in Figure 1.17. In each simulation, the probe traffic is Poisson. In two simulations, the bottleneck link is located between nodes 2 and 5, and in the other four simulations, it is located between nodes 5 and 7. Table 1.11 reports details on the cross traffic in each scenario. In each simulation, there was only one type of cross traffic considered (provided in first column of Table 1.11). Columns 2 and 3 give the total number of flows considered and the number of flows per route, respectively. There are six possible routes in the case that the cross traffic type is either Poisson or On/Off, and there are twelve routes when the cross

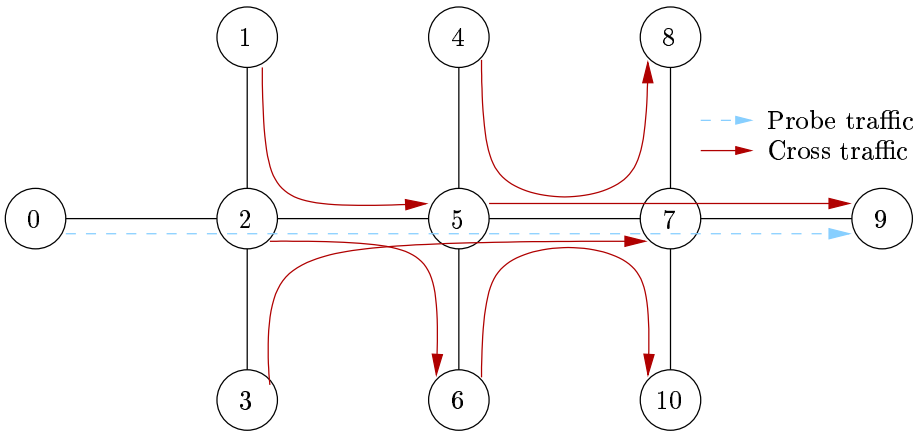

Figure 1.17: The simulated network

Table 1.11: Details on the cross traffic in the simulated scenarios

Along the path			Flows via bottleneck		
Type	Flows	Flows/route	link 2–5	link 5–7	Routes for cross traffic
Poisson	6	1	3	4	$(i, i+4), i = 1, \ldots, 6$
On/Off	750	125		500	$(i, i+4), i = 1, \ldots, 6$
FTP/TCP	1020	85	510	680	$(i, i+4), (i+4, i), i = 1, \ldots, 6$
FTP/TCP	1500	125		1000	$(i, i+4), (i+4, i), i = 1, \ldots, 6$

traffic is the aggregation of 1500 FTP/TCP flows (see column 6). Column 4 (resp. column 5) gives the number of cross traffic flows going through the bottleneck when the latter is the link 2–5 (resp. link 5–7).

We observed in our experiments that the propagation delay is crucial in simulations in which the cross traffic is transported by TCP. That is, of course, because TCP is a closed-loop protocol, as opposed to UDP which is used to transport Poisson or On/Off flows. Table 1.12 reports the relative error (expressed in percentage) returned by scheme P_L_R after 5000 probes only. We notice that $\hat{\lambda}$ performs very well (see column 5 in Table 1.12), which is not the case of $\hat{K}$, as the latter misestimates the buffer size K when the cross traffic is the aggregation of FTP/TCP flows (cf. rows 6–8 in Table 1.12, column 4). Observe that the error on K decreases from 27.6% to 16.8% when the number of FTP/TCP flows increases from 680 to 1000.

Table 1.12: Relative error of $\hat{K}$ and $\hat{\lambda}$ (expressed in %) after 5000 probes

	Flows via bottleneck		Relative error		Propagation
Bottleneck	Type	Flows	$\hat{K}$	$\hat{\lambda}$	delay considered?
link 2–5	Poisson	3	4.6	1.4	No
link 5–7	Poisson	4	5.6	0.6	No
link 5–7	On/Off	500	0.7	2.2	No
link 2–5	FTP/TCP	510	9.5	2.7	Yes
link 5–7	FTP/TCP	680	27.6	0.7	Yes
link 5–7	FTP/TCP	1000	16.8	5.5	Yes

Note that when the cross traffic is transported by TCP, it is necessary to account for the propagation delay in order for the scheme to behave well, thereby, suggesting an extension to the $M+M/M/1/K$ queue model in which the end-to-end delay is the sum of the response time of the queue and a propagation delay. The latter might be constant or a random variable.

1.8 Extensions

1.8.1 From simulation to reality

Till now, we have always assumed to have access to the first n samples of $\{a_i\}_i$, $\{d_i\}_i$, $\{X_i\}_i$ and $\{Y_i\}_i$. In this work, we have carried out simulations to generate traffic traces, and the samples were extracted from the traces. However, ultimately, we must extract the samples from the real network (e.g. the Internet). How can we do this?

Usually, real-time applications use the Real-time Transport Protocol (RTP) [109] together with UDP and IP. RTP provides end-to-end network transport functions suitable for this kind of application, over multicast or unicast network services. RTP consists of two parts, a data part and a control part referred to as RTCP, the RTP Control Protocol. The feedback information is carried in RTCP packets referred to as Receiver Reports (RRs).The rate at which they are multicast is controlled so that the load created by the control information is a small fraction of that created by data traffic. The RR sent by a destination includes several pieces of information: the highest sequence number received, the number of packets lost, the estimated packet interarrival jitter, and timestamps. At the sender, the $\{a_i\}_i$ are available, the $\{d_i\}_i$ are retrieved from the timestamps present in the RR and the $\{X_i\}_i$ are retrieved from the highest sequence number received at the destination, also given in the RR. As for the $\{Y_i\}_i$, they are hard to obtain. In [86], the authors propose an algorithm to estimate the clock skew in network delay measurements. This algorithm can be adapted to estimate the $\{Y_i\}_i$ (mainly, $Y = 0$ if the measured delay is minimal) but this estimation will be weak and uncertain, as the service times are considered constant. Fortunately we found that P_L_R is the best scheme and hence we will not use U. The work assumes a perfect knowledge of the bottleneck capacity. In some cases, μ is known exactly (we know the routes and we know the routers) but sometimes μ is to be estimated and this introduces further error. Its impact still needs to be investigated.

1.8.2 Example of a possible application

An interesting application for the methods proposed in this chapter is routing in content distribution networks. The goal would be to infer the available bandwidth and buffer size of the bottleneck queue on a path between two application layer routers so as to determine how to route new traffic. It should be possible to probe at a sufficiently high rate to quickly obtain good estimates. This could be done by embedding a Poisson stream within the data traffic and/or adding a (relatively) low bandwidth probe stream. Furthermore, between two application layer routers, we expect there to be one bottleneck node residing at a peering point between the two backbone networks within which the routers reside.

1.9 Conclusion

In this work, we have proposed two simple models for a connection, based on a single server queue with finite waiting room, to infer the *buffer size* and the *intensity of cross traffic* at the bottleneck link of a path between two hosts. We have quantified several parameters of both models and obtained eleven pairs of *moment-based* estimators. Using traces generated by the network simulator `ns-2`, estimated values for both parameters have been calculated according to the characteristics of the *a priori* models. Pairs of estimators have been discarded while others have proved to give good results. However, the pair of estimators we have "elected" as the best one need to be tested on an experimental network, or even better, on the Internet, in order to evaluate its performance under realistic network traffic conditions.